Ana Teresa Carrilho Carvalho

Licenciada em Biologia

The mechanism of the *Legionella* VipA protein in altering actin dynamics during infection

Dissertação para obtenção do Grau de Mestre em

Bioquímica para a Saúde

Orientador: Alvaro Crevenna, Doutor, European Molecular Biology Laboratory (EMBL), Rome

Co-orientadores: Irina Franco, Doutora, Faculdade de Ciências e Tecnologia da Universidade Nova de Lisboa (FCT/UNL), e Zachary Hensel, Doutor, Instituto de Tecnologia Química e Biológica da Universidade Nova de Lisboa (ITQB NOVA)

Outubro de 2019

Ana Teresa Carrilho Carvalho

Licenciada em Biologia

The mechanism of the *Legionella* VipA protein in altering actin dynamics during infection

Dissertação para obtenção do Grau de Mestre em

Bioquímica para a Saúde

Orientador: Alvaro Crevenna, Doutor, European Molecular Biology Laboratory (EMBL), Rome

Co-orientadores: Irina Franco, Doutora, Faculdade de Ciências e Tecnologia da Universidade Nova de Lisboa (FCT/UNL), e Zachary Hensel, Doutor, Instituto de Tecnologia Química e Biológica da Universidade Nova de Lisboa (ITQB NOVA)

Júri:

Presidente: Professor Doutor Pedro Manuel Henriques Marques Matias

Arguente: Doutor Pedro Matos Pereira

Vogal: Doutor Zachary Jay Hensel

Instituto de Tecnologia Química e Biológica da Universidade Nova de Lisboa

Outubro de 2019

The mechanism of the *Legionella* VipA protein in altering actin dynamics during infection

Agradecimentos/ Acknowledgments

Agradeço a todos os que, de forma institucional, pessoal, ou ambas, contribuíram para o desenvolvimento deste que foi o projecto mais desafiante e exigente que tive até hoje. A todos, muito obrigada!

Ao ITQB NOVA, pela oportunidade, e ao Doutor Alvaro Crevenna, por me ter aceite no projecto.

Ao Doutor Zach, pela ajuda indispensável em toda a parte de microscopia e de programação, sem a qual não teria chegado ao fim, e por tudo o que me ensinou. Por ter aceitado orientar a minha tese, que lhe caiu nas mãos de um dia para o outro, e pelo empenho e dedicação enormes que pôs nessa função. Pelo bom ambiente no laboratório, no qual adorei trabalhar, e pela calma e pensamento positivo que tantas vezes me transmitiu.

À Doutora Irina, que tanto me ensinou. Pela enorme ajuda no planeamento experimental, e pela rapidez de sempre a resolver as minhas dúvidas. Pelo acompanhamento e apoio que, ainda que vindos de outra instituição, nunca faltaram. Por ter acreditado em mim e no meu trabalho apesar dos contratempos, e pela motivação e entusiasmo que mostrou sempre.

Ao Doutor Jaime Mota e a todas as colegas do *Infection Biology Laboratory* (FCT/UNL), que tão bem me receberam e que se mostraram sempre disponíveis para me ajudar. Ao Doutor Federico Herrera, à Fernanda Murtinheira e ao Ricardo Vilela (*Cell Structure and Dynamics Laboratory*, FCUL), por me terem dispensado o material e parte do seu tempo para me ensinar tudo o que sei sobre trabalhar com células animais. À Doutora Lígia Saraiva e restantes membros do *Molecular Mechanisms of Pathogen Resistance Laboratory* (ITQB NOVA), por me terem permitido a utilização das instalações para cultura de células animais, e ao *Bacterial Imaging Cluster* do ITQB NOVA, que me permitiu a utilização do microscópio confocal.

À Professora Teresa Catarino, que várias vezes me ouviu e soube ouvir. Pela calma e serenidade que me transmitiu quando mais precisei e pelo trabalho exemplar que desempenha enquanto coordenadora do Mestrado.

Aos meus colegas de laboratório, que me mostraram que o companheirismo é a chave para ultrapassar qualquer obstáculo. Obrigada pelos vossos conselhos e por todas as vezes que puxaram por mim. Pelas horas de almoço que muitas vezes se prolongaram em horas do café intermináveis, frequentemente passadas a analisar conteúdos sem qualquer relevância cultural, mas muitas vezes também a desabafar ou a conversar sobre as nossas ambições e projectos para o futuro (às vezes só precisamos de parar e conversar com alguém). Pelas idas aos gelados e as horas do bolo, e pela seriedade quando foi preciso. À Soraia Lopes, pelo exemplo

de perseverança e determinação, que me mostrou que quem se esforça sempre alcança. À Sara Costa, por tudo o que me ensinou, quer a nível profissional, quer a nível pessoal. Por todas as vezes que se sentou ao meu lado a resolver problemas e me acalmou no auge do meu nervosismo, e pela ajuda que me deu sempre que bloqueei enquanto calculava concentrações de reagentes. Pela inspiração que é enquanto mulher (e) cientista, e pela amiga que demonstrou ser ao longo do último ano. Ao Ricardo Quiteres, pela diversão constante que foi trabalhar com ele, e por me explicar tudo aquilo que lhe perguntava, mesmo quando lhe perguntava a mesma coisa várias vezes, qual professor. Por não ter ficado chateado comigo mais do que umas horas quando me esqueci de ligar o fluxo da câmara e lhe atrasei o trabalho, e pela referência que é por aliar a qualidade de bom aluno à de bom colega e amigo.

Aos meus amigos, que têm sempre uma palavra animadora para dizer. Pelo exemplo e a motivação dos que já passaram por esta fase, e pelo apoio mútuo dos que a atravessaram comigo. Pela amizade de sempre, mesmo quando os encontros não são os de sempre.

À minha família, com quem tenho o enorme privilégio de poder contar. Por acreditarem em mim e por me fazerem acreditar em mim. Por todo apoio e força que me deram ao longo deste ano, e pelo respeito que mostraram sempre pelo meu trabalho.

Ao Kiko, que me consolou nos piores momentos e celebrou comigo todos os sucessos. As conquistas não teriam o mesmo sabor se não as pudesse celebrar com ele.

Aos meus pais, que tornam tudo possível.

"My dear, here we must run as fast as we can, just to stay in place. And if you wish to go anywhere you must run twice as fast as that."

Lewis Carroll, *Alice in Wonderland & Through the Looking Glass* (1871)

"Caminante, no hay camino,
se hace camino al andar".

Antonio Machado, *Proverbios y cantares (XXIX)* in *Campos de Castilla* (1912)

This work was partially supported by PPBI - Portuguese Platform of BioImaging (PPBI-POCI-01-0145-FEDER-022122), co-funded by national funds from OE - "Orçamento de Estado" and by european funds from FEDER - "Fundo Europeu de Desenvolvimento Regional"

Resumo

A bactéria *Legionella pneumophila* é facultativamente intracelular e encontra-se frequentemente em pontos de água doce e nos solos, onde é capaz de parasitar uma grande variedade de protozoários. Mecanismos de co-evolução conferiram-lhe a capacidade de parasitar outras células fagocíticas e de se tornar potencialmente patogénica em humanos. Após a inalação pelo hospedeiro de aerossóis contaminados, *L. pneumophila* consegue sobreviver e replicar-se dentro dos macrófagos pulmonares através da criação de um fagossoma especializado que não é passível de ser degradado, podendo levar ao desenvolvimento da pneumonia conhecida como Doença dos Legionários. Através de um sistema de secreção do tipo IV, a bactéria injecta proteínas efectoras na célula hospedeira e desta forma perturba ou aproveita-se de diversos processos celulares. O efector VipA interfere com processos de transporte vesicular em levedura e apresenta co-localização com actina em vários modelos celulares. Ensaios anteriores revelaram também que esta proteína atua como factor de nucleação de actina *in vitro*. No presente trabalho complementou-se ensaios prévios recorrendo à visualização de polimerização de actina *in vitro* usando microscopia de fluorescência de campo-amplo. Observou-se que a adição de profilina, proteína que forma complexos com a actina monomérica em células eucarióticas, diminui, porém não bloqueia, a nucleação de actina mediada por VipA. Verificou-se ainda que este efector tem a capacidade de promover a nucleação de actina na presença de Rab5, um marcador de endossomas primários, e ensaios baseados em microscopia confocal de fluorescência apresentaram elevada co-localização entre VipA e Rab5 em células HeLa. Apesar de a proteína VipA possivelmente não ser essencial à sobrevivência e replicação intracelulares de *L. pneumophila*, a sua acção concertada na modulação da rede actínica e na disrupção da via endocítica na célula hospedeira pode contribuir para a formação do vacúolo especializado que alberga estas bactérias.

Palavras-chave: *Legionella pneumophila*; efector bacteriano; VipA; actina; nucleador; via endocítica.

Abstract

Legionella pneumophila is a facultative intracellular bacterium that is commonly found in fresh water and soils, parasitizing a wide range of protozoa hosts. Co-evolution mechanisms allowed this bacterium to parasitize other phagocytic cells and rendered it the ability to become a potential human pathogen. For instance, after inhalation of contaminated aerosols by the host, it can survive and replicate inside human macrophages in the lungs by creating a specialized phagosome that is not degraded, possibly resulting in the severe pneumonia known as Legionnaires' disease. *L. pneumophila* relies on a type IV secretion system to inject effector proteins into the host cell to disrupt or take advantage of several cellular processes. The VipA bacterial effector was found to interfere with vesicular trafficking in yeast and to colocalize with actin in several cellular models. Moreover, previous bulk assays revealed that it acts as an actin nucleator *in vitro*. In this work we complemented previous assays by visualizing actin polymerization *in vitro* through widefield fluorescence microscopy. We found that the addition of profilin, a protein found in complex with monomeric actin in eukaryotic cells, decreases but does not block VipA-mediated actin nucleation. Furthermore, the effector was able to enhance actin nucleation in the presence of Rab5, a marker of early endosomes, and confocal fluorescence microscopy assays showed strong colocalization between VipA and Rab5 in HeLa cells. Although VipA is possibly not essential for the intracellular survival and replication of *L. pneumophila*, its concerted action in actin network modulation and endosome trafficking disruption in the host cell may contribute to the formation of the *Legionella*-containing vacuole.

Keywords: *Legionella pneumophila*; bacterial effector; VipA; actin; nucleator; endocytic pathway.

General contents

Figure contents

Table contents

List of abbreviations

ABP – Actin-binding protein;
ADP/ATP – Adenosine diphosphate/ adenosine triphosphate;
ALP – Alkaline phosphatase;
APS – Ammonium persulfate;
Arp – Actin-related proteins;
BSA – Bovine serum albumin;
CHO – Chinese hamster ovary;
CPS – Carboxypeptidase S;
CPY – Carboxypeptidase Y;
CPY-Inv – Carboxypeptidase Y-Invertase;
DeLTA – Deep learning for time-lapse analysis;
DMEM – Dulbeco's modified Eagle's medium;
DMI – Discrete Molecular Imaging;
DPBS – Dulbecco's phosphate buffered saline;
ECDC – European Center for Disease Prevention and Control;
EEA – Early endosome antigen;
EGFP – Enhanced green fluorescent protein;
EL – External light;
EMCCD – Electron multiplier charge-coupled device;
ER – Endoplasmic reticulum;
ESCRT – Endosomal sorting complex required for transport;
EU/EEA – European Union / European Economic Area;
FBS – Fetal bovine serum;
GAP – GTPase activator protein;
GEF – Guanine nucleotide exchange factor;
GFP – Green fluorescent protein;
GST – Glutathione S-transferase;
GTP – Guanine triphosphate;
GTPase – Guanine triphosphate hydrolase:
HCP UV – High-sensitive Ctcp plate ultraviolet;
HGT – Horizontal gene transfer;
HOPS – hsp170-hsp90 organizing protein;
Icm/Dot – Intracellular multiplication/ defective organelle trafficking;
IMAC – Immobilized metal affinity chromatography;
IPTG – Isopropyl β- d-1-thiogalactopyranoside;
LAMP – Lysosomal-associated membrane protein;
LB – Lysogeny broth;
LC/MS – Liquid chromatography/ mass spectrometry;

LCV – *Legionella*-containing vacuole;

LDL – Low-density lipoprotein;

LMW – Low molecular weight;

LSM – Laser scanning microscopy;

MVB – Multi vesicular body;

MWCO – Molecular weight cut-off;

NPF – Nucleation promoting factor;

NS – Non-Ig secreting;

NTA – Nitrilotriacetic acid;

PBS – Phosphate buffered saline;

PCR – Polymerase chain reaction;

PEPSY – Pathogen effector protein screening in yeast;

PIP – Phosphoinositide;

PMSF – Phenylmethylsulphonyl fluoride;

PMT – Photo-multiplier tube;

SDS-PAGE – Sodium dodecyl sulphate polyacrylamide gel electrophoresis;

SNARE – Soluble NSF (N-ethylmaleimide-sensitive factor) attachment protein receptor;

T4SS – Type IV secretion system;

TEMED – Tetramethyl ethylenediamine;

VCA – Verprolin, cofilin, acidic;

Vip – VPS inhibitor protein;

VPS – Vacuolar protein sorting;

WASP – Wiskott-Aldrich syndrome protein;

WAVE – WASP-family verprolin-homologous protein;

WHO – World Health Organization;

1. Introduction

1.1. Legionnaires' disease

Legionnaires' disease is a form of severe pneumonia caused by the *Legionellae* group of bacteria, with the freshwater species *Legionella pneumophila* responsible for most reported cases of infection according to the World Health Organization (WHO) (World Health Organization, 2018). The severe, multi-system disease involves a pneumonic form, in which patients may experience fever, non-productive cough, headache, myalgia, rigor, dyspnea, diarrhea and delirium. Legionellosis may have two other clinical presentations: Pontiac fever, a self-limited flu-like illness which usually lasts for 2–5 days, and a completely asymptomatic form (Fields et al., 2002).

The *Legionella* genus was established in 1979 and was traced to *L. pneumophila*, a previously unrecognized bacterium. It was named after the disease, which was in turn named after a large outbreak occurred three years before. In the summer of 1976, the celebration of the bicentennial anniversary of the Declaration of Independence was taking place in Philadelphia. Altogether, 182 members of the Pennsylvania American Legion developed an acute respiratory illness that culminated in 29 deaths after returning from the convention. At the time, newspapers reported the occurrence of an epidemic of a mysterious fatal disease resembling influenza clinical pattern (Winn, 1988).

Transmission of the disease is usually by inhalation of contaminated aerosols or aspiration of contaminated water, except for *Legionella longbeachae* infection, which is thought to be contracted by exposure to contaminated potting compost or soil (Lindsay et al., 2012). Large outbreaks have been associated with contaminated cooling towers, hot- and cold-water systems, and whirlpool spas. Fountains, supermarket mist machines and ice machines have also been associated with Legionnaires' disease (Barrabeig et al., 2010; Bencini et al., 2005; Bennett et al., 2014; Den Boer et al., 2002; Colville et al., 1993; García-fulgueiras et al., 2003; Greig et al., 2004; O'Loughlin et al., 2007). To date, only one evidence of person-to-person transmission has been verified. It occurred during the second largest outbreak of the disease recorded internationally, which took place in 2014 in Vila Franca de Xira, a Portuguese industrial town, leading to 403 identified cases, 377 of which were later confirmed, and accounting for 14 deaths. Laboratorial assays revealed a new strain of *L. pneumohila* as the causative agent, and the source of the outbreak was traced back to a cooling tower of a local industry (Borges et al., 2016).

Throughout the years there has been a debate as to whether the only manifestation of such disease is pneumonia. This open question is of high relevance as it is not possible to clinically distinguish patients with Legionnaires' disease from patients with pneumonias caused by other agents, requiring laboratory analysis (Fields et al., 2002). For several decades, serology was used as the consensus diagnosis technique. Despite being a fairly sensitive and specific primary diagnostic method, controversies have emerged, and, from the mid-1990s, urine antigen detection became widely accepted as routine diagnosis method, recently accounting for

70–80% of diagnosed cases in Europe and in the United States of America, although it displays some limitations as well (Harrison et al., 1987; Helbig et al., 2003; Plouffe et al., 1995; Svarrer et al., 2012). Culture and isolation from clinical specimens allow epidemiological typing, providing valuable data for control and prevention. However, it is considered too time consuming and costly to be implemented in routine diagnosis and rapid recognition of outbreaks (Phin et al., 2014). Real-time PCR is now the molecular method of choice for detection of *Legionella spp*, offering specificity, sensitivity and rapidity, and it is being strongly encouraged for early diagnosis (Mentasti et al., 2012).

Therapy for Legionnaires' disease consists in antibiotic administration and management of possible complications and comorbidities (Cunha, 2008). Early diagnosis and treatment with the effective antibiotics are a priority since in such case recovery is most likely, and untreated disease presents high levels of mortality and morbidity. The β-lactam antibiotics, used to treat bacterial community-acquired pneumonias, are in this case ineffective (Chidiac et al., 2012; Levy et al., 2010). Successful treatment depends on antibiotics that achieve therapeutic intracellular concentrations inside alveolar macrophages; these include the macrolides, fluoroquinolones and cyclin families (Garau et al., 2010; Garrido et al., 2005; Griffin et al., 2010; Haranaga et al., 2007; Mandell et al., 2007; Mykietiuk et al., 2005).

According to the WHO, Legionnaires' disease is believed to occur worldwide, but since many countries lack the proper methods for diagnosis, its actual rate of occurrence is unknown, and its incidence varies according to the level of surveillance and reporting. Data from 2018 report that, of the overall notified cases, around 80% of the victims are over 50 years old, and between 60 and 70% are male. Besides age and gender, other risk factors for community-acquired and travel-associated legionellosis are smoking, history of heavy drinking, pulmonary-related illness, immune-suppression and chronic respiratory or renal illnesses. Regarding hospital-acquired disease, main risk factors include recent surgery, intubation, mechanical ventilation, presence of nasogastric tubes and the use of respiratory therapy equipment, with the immuno-compromised patients being the most susceptible hosts (World Health Organization, 2018). The Annual Epidemiologic Report for 2017 emitted by the European Center for Disease Prevention and Control (ECDC) indicates that Legionnaires' disease remains uncommon and mainly sporadic in the EU/EEA. However, between 2013 and 2017, the overall notification rate increased continuously from 1.2 to 1.8 per 100,000 (ECDC, 2019). Data from 2011 reported a 10% average fatality rate of the disease in Europe (ECDC, 2013).

1.2. *Legionella pneumophila*

1.2.1. General features of the *Legionella* genus

Legionella pneumophila is a Gram-negative bacterium that, together with other species, such as *Legionella longbeachae* and *Legionella micdadei*, belongs to the *Legionella* genus. All the three species have been described as accidental human pathogens. The *Legionellales*

order is composed of intracellular bacteria of the γ-proteobacteria class. These are Gram-negative, non-spore forming, rod-shaped bacteria, and are classically divided into two families: *Legionellaceae*, which comprises the *Legionella* genus, and *Coxiellaceae* (Graells et al., 2018). The *Legionella* genus comprises over 60 species, mostly harmless environmental species. The genomes of nearly the entire *Legionella* genus have been already sequenced (Gomez-Valero and Buchrieser, 2019).

Legionella are facultative intracellular bacteria found in freshwater reservoirs and in soils. Certain species are able to parasitize free-living protozoa, such as *Acanthamoeba castellanii*, *Verbamoeba veriformis* or *Hartmanella veriformis*, in aquatic environment (Rowbotham, 1980).

1.2.2. From protozoa to human cell hosts

Sustained horizontal gene transfer (HGT) events within the protozoan niche may have allowed *L. pneumophila* to become a parasite of human phagocytic cells. In fact, upon inhalation of contaminated aerosols, it can infect and replicate in alveolar macrophages in the lungs, leading to inflammation and potentially resulting in disease (Franco et al., 2009). Acquisition of host DNA by pathogens due to their natural competence has influenced co-evolution over millions of years, and allows the recipient species to improve their fitness, resulting in the development of pathogenicity or virulence traits. Co-evolution between *L. pneumophila* and its natural hosts in aquatic environments is one of the few reported cases of eukaryote-to-prokaryote HGT (Gomez-Valero and Buchrieser, 2019).

Around 5% of the proteins encoded in the *L. pneumophila* genome correspond to proteins with eukaryotic-like motifs or that display eukaryotic-like properties. This finding suggested that these bacteria could secrete these proteins inside the host cell (Gomez-Valero and Buchrieser, 2019). Indeed, the *L. pneumophila* genome also encodes a type IVB secretion system (T4BSS) which is responsible for the translocation of over 300 bacterial effectors (Lifshitz et al., 2013). A bacterial “effector” is any protein translocated from pathogenic bacteria into the host cell that can interfere with host cellular processes. These proteins are responsible for pathogenic traits in infectious bacteria (Franco et al., 2009). A type II secretion system was also found to promote translocation of some bacterial effectors into both its natural and accidental hosts (Debroy et al., 2006). Importantly, secreted *Legionella* effectors studied to date revealed none or almost no defect on bacterium intracellular growth when deleted, indicating a high degree of redundancy (Gomez-Valero and Buchrieser, 2019).

The versatile repertoire of *Legionella* effectors comprises a variety of proteins able to interfere with a wide range of host cellular processes. For instance, *L. pneumophila* effectors have been found to interact with small GTPases of the early secretory pathway. This is the case of RalF, that recruits and activates Arf1, a small GTPase involved in vesicle budding and retrograde transport in eukaryotes. Interestingly, the *Legionella* genus displayed the unique feature of encoding over 180 predicted small GTPases, including Rab GTPases, which are master regulators of intracellular membrane trafficking in eukaryotes (Zhen and Stenmark, 2015). Other *Legionella* effectors have displayed the ability to exploit host signaling pathways

by binding to phosphoinositide lipids. RomA, a *L. pneumophila* effector that contains an eukaryotic domain, has been found to induce a unique host chromatin modification (Rolando et al., 2013). Furthermore, other *Legionella* effectors, such as LegA8, AnkN, or AnkX, have been implicated in microtubule-dependent vesicle transport, and others such as VipD, LegC2, or LegC7, target the secretory and endosomal pathways at different levels and through diverse mechanisms. The repertoire of *Legionella* effectors displays high plasticity both between species, with a core of only eight conserved effectors, and between bacterial strains, with less than 80% of the effector encoding-genes of the Philadelphia1 strain shared by the Paris, Lens, and Corby strains (reviewed in Franco et al., 2009, and Gomez-Valero and Buchrieser, 2019).

The ability to take up genetic material from eukaryotic hosts presumably confers a selective advantage to these bacteria. This ability may be the key in *L. pneumophila* to occupying the niche as a parasite of phagocytic cells, such as human lung macrophages. Although some of its effectors may have arisen through convergent evolution, HGT as a consequence of eukaryotic parasitism is the major source of effectors (Franco et al., 2009).

1.2.3. Intracellular life cycle of *L. pneumophila*

Legionella pneumophila grows within a wide range of phagocytic host cells, ranging from freshwater amoebae to mammalian macrophages (Gao et al., 1997). It is able to multiply in human blood monocytes and human alveolar macrophages, and under culture conditions such multiplication is exclusively intracellular. Studies carried out in human monocytes revealed that the formation of a specialized *L. pneumophila* phagosome entails a sequence of cytoplasmic events that take place during the first 8 hours after phagocytosis (Horwitz, 1983a). This process involves the interaction between the phagocytic vacuole and monocyte smooth vesicles, mitochondria and ribosomes, and results in the formation of the so-called *Legionella*-containing vacuole (LCV). This modified phagocytic vacuole does not fuse with lysosomes and displays a near neutral pH. It has been demonstrated that *L. pneumophila* inhibits phagosome-lysosome fusion (Horwitz, 1983b), a trait shared with other intracellular human pathogens such as *Toxoplasma gondii* (Jones and Hirsch, 1972), *Mycobacterium tuberculosis* (Armstrong and Hart, 1971), and *Chlamydia psittaci* (Friis, 1972). It was observed that the bacterium also inhibits the typical acidification known to occur in lysosomes and phagolysosomes. One possible explanation for this is that the inhibition of the phagosome-lysosome fusion may avoid LCV acidification (Horwitz and Maxfield, 1984).

Internalization of *L. pneumophila* follows attachment to complement receptors and engulfment by either a single pseudopod that coils around the bacterium (Horwitz, 1984) or by conventional phagocytosis (Rechnitzer and Blom, 1989). During the first hour of infection, host ER vesicles fuse with the membrane of the LCV, which starts to be surrounded by mitochondria as well. Four hours post-infection, fewer smooth vesicles and mitochondria are surrounding the vacuole, which begins to be strongly associated with ribosomes. By 4 to 10 hours after phagocytosis, the bacterium begins to multiply inside this compartment with a doubling time of approximately 2 hours. Bacteria multiply inside the ribosome-lined vacuole until hundreds of

organisms fill it (Horwitz, 1983a). Eventually, bacteria are released either by lysis of the host cell (Wiater et al., 1998) or by a non-lytic exocytic pathway as demonstrated for some protozoan hosts (Chen et al., 2004), and are then able to undergo new cycles of infection or parasitism. Survival and replication of *L. pneumophila* inside lung macrophages disturbs the adaptive immune response by interfering with antigen presentation, allowing the bacteria to escape the host's immune system (Bugalhão et al., 2016).

Vacuoles containing replication-competent *L. pneumophila* have been shown to have limited early interactions with the host endocytic pathway. Furthermore, it is known that these bacteria avoid fusion between the LCV and the lysosome by disrupting maturation before fusion with the late endosomes of the endocytic pathway in eukaryotic cells (Roy et al., 1998). Such modulation of phagosome transport is coordinated by the T4BSS protein complex, which secretes the responsible bacterial effector proteins directly into the host cell (Kagan and Roy, 2002; Wiater et al., 1998).

1.3. The *Legionella* Type IVB Secretion System

The *L. pneumophila* genome encodes 27 *icm*/*dot* genes, found to be essential for bacterial intracellular survival and replication in all its hosts. These genes were named after the observed functions and *icm* and *dot* stand for **i**ntra**c**ellular **m**ultiplication and **d**efective **o**rganelle **t**rafficking, respectively. These are located in two unlinked loci and encode the T4BSS protein complex that mediates translocation of bacterial effector proteins into the host cell (Franco et al., 2009; Lifshitz et al., 2013; Marra et al., 1992; Purcell and Shuman, 1998; Sadosky et al., 1993; Segal et al., 1998; Vogel and Isberg, 1999; Vogel et al., 1998). These genes act early during the formation and establishment of the LCV and appear to control its properties (Wiater et al., 1998).

The Icm/Dot (T4BSS) apparatus is a complex of *L. pneumophila* proteins that, together, constitute a channel between the bacterium and the host cytosol. These components have specific locations and display a wide range of functions. Five Dot components (DotC, DotD, DotF, DotG and DotH) have been implicated in the formation of the complex that connects the inner and outer membranes of the bacterial envelope, with DotH possibly involved in the formation of the continuous channel that links the outer membrane to the host endosomal membrane. Other identified Icm and Dot proteins are either bacterial cytoplasmic components or accessory factors of the bacterial inner membrane and participate in regulation processes required for the proper function of the system. DotL, for instance, is an ATPase that associates with the major core to prepare translocation of proteins. IcmS associates with other bacterial proteins to coordinate the presentation of the translocated substrates (reviewed in Isberg et al., 2009) .

Delivery of effector proteins is a process widely used by bacterial pathogens to subvert host cell functions. Such delivery is performed by complex devices that can be triggered by environmental stimuli. The *Legionella* Icm/Dot system can only be triggered by the target host cell, with phagocytosis required to initiate the intimate contact necessary for the translocation of

effector molecules. It has been hypothesized that this may be an intrinsic mechanism through which *L. pneumophila* tests the fitness of the potential host cell, preventing effector delivery into non-productive cells (Charpentier et al., 2009).

1.4. Alteration of *S. cerevisiae* trafficking pathways by *L. pneumophila* bacterial effectors

The amenability for genetic manipulation and the existence of an extensive library of mutants and strains expressing fluorescently labeled proteins facilitates studying bacterial effectors in *Saccharomyces cerevisiae*. Due to the conserved organelle trafficking pathways between *S. cerevisiae* and higher eukaryotes, and their shared complex intracellular organization, this model organism allowed researchers to overcome the ineffectiveness of classical forward and reverse genetics approaches in *L. pneumophila* hosts when it comes to the study and functional characterization of *L. pneumophila* effectors (Franco et al., 2012). Such ineffectiveness is likely due to high functional redundancy among effectors and/or host cell target proteins or pathways, and species specificity of their functions (Chen et al., 2007; Luo and Isberg, 2004; O'Connor et al., 2011). Studies in *S. cerevisiae* allowed the identification of eukaryotic trafficking pathways and regulatory proteins, and of most known bacterial effector proteins (Feyder et al., 2015). Furthermore, many bacterial effectors normally involved in mammalian infection have been shown to retain their biological function in yeast (Lesser and Miller, 2001; Valdivia, 2004).

After transport from the endoplasmic reticulum to the Golgi apparatus, newly synthesized proteins are transported to the growth medium, to the plasma membrane, or to the yeast vacuole, for either degradation or redirection to the recycling pathway. Sorting to the vacuole occurs via the alkaline phosphatase (ALP) pathway in an endosome-independent fashion, or via the vacuolar protein sorting (VPS) pathway, through endosomes that end up fusing with the vacuole (Cowles et al., 1997; Feyder et al., 2015). Several yeast regulatory proteins that concentrate cargo and ensure the recruitment of additional coating proteins to form vesicles in the trans-Golgi were identified and designated as Vps effectors (Bowers and Stevens, 2005; Feyder et al., 2015; Raymond et al., 1992). Carboxypeptidase Y (CPY) is a well-known soluble vacuole-targeted pro-enzyme that follows the VPS pathway (Raymond et al., 1992). Cytoplasmic membrane proteins require an additional step since they need to be first sorted into vesicles that fuse with the late endosome or multivesicular body (MVB). The initial inward budding depends on a specific protein machinery mainly composed by class E Vps proteins which assemble into four different complexes called endosomal sorting complex required for transport (ESCRT). One of the most studied yeast molecules that undergo the MVB pathway is the transmembrane protein carboxypeptidase S (CPS) (Feyder et al., 2015; Shohdy et al., 2005).

Several trafficking pathways in *S. cerevisiae*, such as the MVB pathway, are controlled by components of the VPS pathway. Some of these protein components have orthologs in mammalian cells, which play similar roles in the endocytic pathway (Babst et al., 2000;

Siddhanta et al., 1998). Pathogen effector protein screening in yeast (PEPSY) carried out in *S. cerevisiae* led do the identification of three *L. pneumophila* effectors that interfere with the VPS trafficking pathways (Shohdy et al., 2005). This methodology took advantage of the hydrolase carboxypeptidase Y-Invertase (CPY-Inv), a hybrid vacuole-targeted protein expressed by the NSY01 reporter yeast strain, which due to the presence of the invertase portion localizes at the cell surface. When normal trafficking is impaired, cargo vesicles are prevented from reaching the vacuole leading to missorting of this protein and to its referral into vesicles destined to the cell surface, resulting in its aberrant secretion. By means of a particular screening medium, the Vps^- phenotype can be identified by the presence of a brown precipitate. The wild-type, Vps^+ phenotype, is characterized by white colonies (Darsow et al., 2000; Shohdy et al., 2005).

The expression of three different *L. pneumophila* genes caused a Vps^- phenotype in yeast. These were designated as *vipA*, *vipD* and *vipF*, as they encode **V**ps **i**nhibitor **p**roteins. Effects of *vip* genes expression on yeast trafficking were characterized by detailed analysis of proteolytic maturation of yeast proteins via the three above mentioned major yeast trafficking pathways. VipA expression resulted in the partial accumulation of precursor CPY and CPS, indicating an impairment of trafficking between either the Golgi and the late endosome, or the late endosome and the vacuole, and no detectable effect on ALP. Additionally, these proteins were found to be Icm/Dot (T4BSS) substrates (Shohdy et al., 2005).

1.5. The *Legionella pneumophila* VipA bacterial effector

1.5.1. General features of the VipA protein

Assays consisting of the transgenic expression of VipA-GFP fusions in *S. cerevisiae* followed by confocal fluorescence microscopy analysis revealed that VipA localizes in puncta in yeast cells, whereas VipA-1, a mutant with an in-frame insertion in the *vipA* gene that disrupts the bacterium's ability to cause a Vps^- phenotype in the PEPSY assay, displays a homogeneous cytosolic distribution. Consistently, infection of TPH-1 human macrophages with a wild-type *L. pneumophila* strain revealed the presence of VipA in diverse structures inside the host cell, varying in size from puncta to larger formations. Additionally, the effector was not found to be associated with the LCV at any time-point of a 14-hour infection process. Infection with a mutant *L. pneumophila* strain harboring a plasmid encoding VipA-1, despite leading to similar levels of translocated effector into the host cell, exhibited homogenous cytosolic distribution of the effector. Moreover, this VipA subcellular localization was found to be independent of the translocation of other *Legionella* effectors after transgenic expression in a Chinese hamster epithelial cell line (CHO) (Franco et al., 2012).

Infection of human macrophages and the amoeba *A. castellanii* revealed that entry and replication *of L. pneumophila* inside these hosts is not affected by VipA deletion (Franco et al., 2012). This observation is common to the vast majority of the over 300 T4BSS-dependent *L.*

pneumophila effector proteins that are translocated into the host cell, which yield no obvious phenotype when their encoding genes are deleted (Zhu et al., 2011).

The primary structure of this effector does not present significant similarities to known proteins or domains. It has nonetheless a predicted coiled-coil (CC) region (from amino acid residue F_{133} to T_{206}), a motif known to be involved in protein-protein interactions (Mier et al., 2017). Two other motifs were identified in the VipA structure, and are known to be involved in the capacity of several bacterial and mammalian proteins to modulate actin dynamics: an Aspargine-Proline-Tyrosine motif (NPY_{76-78}) and a proline-rich region ($P_{253-262}$) (Brady et al., 2007; Gertler et al., 1996; He et al., 2009).

Previous work aimed at identifying the contributions of the major regions of VipA to its subcellular localization and functions led to the generation of several VipA constructs. Transient expression of EGFP-fusions of these constructs in CHO mammalian cells showed that the presence of only the N-terminal (NH_2) region (amino acid residues M_1 to F_{133}), the C-terminal (COOH) region (residues T_{206} to L_{339}), or the coiled-coil region, resulted in a homogeneous cytosolic distribution (Bugalhão et al., 2016).

1.5.2. VipA acts as an actin nucleator *in vitro*

Pull-down assays followed by LC/MS identified β-actin as a eukaryotic binding partner of the *Legionella* VipA protein and showed that VipA binds actin without the requirement of any additional factors. Moreover, pyrene-actin polymerization assays that measure the overall fluorescent signal in real-time revealed that VipA enhances actin polymerization *in vitro* in a concentration-dependent manner and without the requirement of additional proteins until a saturation level is reached (Franco et al., 2012).

Actin polymerization is a biochemical process in which actin hydrolyses ATP upon polymerization, creating a difference between the critical concentration (C_c) of the more dynamic ATP-bound barbed end (+) and the less dynamic ADP-bound pointed end (-). In eukaryotic cells, monomeric (G) and polymeric (F) actin interact with a large repertoire of proteins that organize filaments into higher-order structures, such as stress fibers, dendritic lamellar arrays, cortical networks, filopodial bundles, contractile rings, among others, that ultimately constitute the actin cytoskeleton. In some conditions, polymerization of the barbed end and depolymerization of the pointed end of the filament occur at the same rate. Such balance between polymerization and depolymerization at the steady state is responsible for the fact that, on average, the filament moves forward keeping the same length. This motion is called “treadmilling”. Therefore, actin acts as a motor system *in vivo*. *In vitro*, actin filaments move towards the direction of the barbed end in the presence of ATP and without the requirement of other proteins, through polymerization and depolymerization in the barbed and pointed ends, respectively. However, treadmilling of pure actin is too slow to account for cell locomotion, where the presence of cooperative proteins is necessary (Bugyi and Carlier, 2010; Le Clainche and Carlier, 2008; Narita, 2011).

The process of actin assembly consists of two steps with different kinetics. It initiates with actin nucleation and is followed by elongation, with nucleation being the rate-limiting step in *de novo* filament formation. Spontaneous nucleation is highly inefficient because it requires sequential formation of actin dimers and trimers, which are highly unstable intermediates that dissociate very rapidly. An actin nucleator is defined as a factor that stimulates the formation of a filament that grows rapidly at its barbed end and that is able to efficiently seed polymerization from a pool of profilin-bound actin monomers, the dominant species of available ATP-actin monomers in eukaryotic cells (Chesarone and Goode, 2009).

Once nucleated, filaments elongate at their fast-growing barbed end, at a rate that is linearly proportional to the concentration of available monomers. Actin nucleators are molecules that respond to cellular signals and regulate the precise timing and location of filament formation, whereas elongation factors, on the other hand, control the extent of filament growth by protecting barbed ends from capping proteins and influencing the rate of subunit addition. Cells are able to construct different actin networks by the control of specific combinations of these factors, resulting in specialized architectures and functions. Responsive and rapid control of actin assembly at specific subcellular locations is at the basis of many cellular processes, such as cell motility, endocytosis, and cytokinesis (Chesarone and Goode, 2009).

Profilin is a major coordinator of F-actin polarized growth that binds to the barbed face of G-actin with high affinity and to F-actin at its barbed end with significant lower affinity. At a low concentration, sufficient to form profilin-actin complexes, it supports filament growth at the barbed end. However, at high concentrations, the higher affinity for monomeric actin enhances filament disassembly. Moreover, it competes with barbed end cappers, trackers, destabilizers and filament branching machineries to regulate filament length fluctuations (Pernier et al., 2016). Profilin is able to sequester actin monomers and thus reduce their availability for polymerization. Yet, the profilin-ATP-actin complex can interact with the barbed end of filaments, releasing the ATP-actin monomer into the filament (Carlsson et al., 1977; Krishnan and Moens, 2009; Witke, 2004), which compensates for the extensive disassembly events and allows filament growth (Pernier et al., 2016).

The concentration of polymerizable actin monomers in cells results from the regulated cycles of assembly and disassembly of actin filaments, and profilin was found to orchestrate such actin homeostasis, generating a pool of polymerizable monomeric actin. In fact, these proteins are able to replenish the pool of ATP-actin monomers by increasing the rate of nucleotide exchange by 1000-fold, which results in an increasing of the polymerization rate (Goldschmidt-Clermont et al., 1992). Studies have linked profilin to a plethora of physiological and pathological processes. For instance, it has been linked to signaling pathways due to its interaction with phosphoinositide molecules (PIPs), and to membrane trafficking processes, given its interaction with proline-rich domain-containing proteins (Krishnan and Moens, 2009). Moreover, intracellular pathogens such as *Listeria monocytogene*s polymerize actin in the host cell to propel themselves through the cytoplasm and to directly spread to neighboring cells, and

the recruitment of profilin by the membrane protein ActA is important for this type of motility (Kocks et al., 1992).

To date, several actin nucleators have been identified and three mechanisms of action have been described. The Arp2/3 complex was the first nucleator being identified. It associates to a nucleation promoting factor (NPF) and catalyzes polymerization of a new filament from the side of an already existing one, resulting in a branched structure. Such mechanism of action is called structural mimicry of polymerization intermediates. The most well-known NPFs of the Arp2/3 complex are the WASP/WAVE family proteins, which induce conformational changes that bring the actin-related subunits into a closer register, possibly mimicking an actin dimer, and afterwards recruit one or two monomers. Formins are nucleators that catalyze the formation of linear filaments *in vitro* by a second process, in which spontaneously formed dimeric or trimeric intermediates are stabilized. *In vivo*, they are responsible for the assembly of diverse structures, such as stress fibers, cytokinetic rings and actin cables (Pollard, 2007). Spire, Cordon bleu (Cobl) and Leimodin (Lmod) were found to nucleate actin by means of a third mechanism, consisting of the recruitment and alignment of actin monomers to form a polymerization seed (Ahuja et al., 2007; Bosch et al., 2007; Chereau et al., 2008; Chesarone and Goode, 2009).

In bulk, *in vitro* pyrene-actin polymerization assays, a significantly shorter lag phase in the overall actin polymerization in the presence of VipA was consistent with a role of VipA in enhancing actin nucleation rather than in increasing the actin elongation rate. Furthermore, the same assay was performed using previously polymerized actin seeds and demonstrated that the effect mediated by this effector during elongation could not account for the overall increase, supporting the idea that VipA acts predominantly as an actin nucleator. The observed effect of VipA on actin polymerization was not as potent as the effect of the Arp2/3 complex activated by the NPFs WASP-VCA or the mouse formin mDia2. Moreover, it did not activate Arp2/3-mediated nucleation, excluding the possibility of VipA mimicking an Arp2/3 NPF (Franco et al., 2012).

Polymerization assays carried out with VipA variants showed that $VipA_{\Delta COOH}$ failed to promote actin polymerization at the concentration in which the highest effect had been previously observed. At such concentration, $VipA_{\Delta NH2}$ nucleates actin as well as $VipA_{WT}$, and $VipA_{\Delta CC}$ is a slightly weaker nucleator. However, at a 10-fold higher concentration, inhibition of polymerization was verified for both $VipA_{\Delta NH2}$ and $VipA_{\Delta CC}$, indicating that the C-terminal region is essential but not sufficient for the ability of the effector protein to mediate actin polymerization *in vitro* (Bugalhão et al., 2016).

Targeting of host cell actin as a mean for successful infection is a strategy widely used between bacterial pathogens. Intracellular bacteria such as *Listeria monocytogenes* and *Shigella* rely on ActA and IcsA bacterial effectors, respectively, to do so (Egile et al., 1999; Kocks et al., 1992), and extracellular *E. coli* requires the Tir protein to interfere with the host actin cytoskeleton (Gruenheid et al., 2001). The *L. pneumophila* protein effector repertoire comprises over 300 proteins. At least five T4BSS substrates modulate actin dynamics, with Ceg14, LegK2, RavK, and WipA inhibiting actin polymerization (Guo et al., 2014; He et al.,

2019; Liu et al., 2019; Michard et al., 2015), and VipA enhancing such polymerization (Franco et al., 2012).

1.5.3. VipA interacts with components of the endocytic pathway

The VipA-derived interference in organelle trafficking in yeast is related to the MVB pathway, and results in an abnormal pre-vacuolar compartment similar to the one characteristic of class E *vps* mutants, in which endocytosed cargo does not fuse completely with the vacuole (Odorizzi et al., 1998; Raymond et al., 1992; Shohdy et al., 2005).

MVBs are present in the endocytic pathway, where extracellular molecules are internalized and sorted at the early endosome between those targeted for degradation into the vacuole/lysosome, after maturation into late endosomes, and those to follow a recycling pathway (Feyder et al., 2015). During endocytosis, cargo sorted for degradation is selectively packaged into regions of the early endosome that exhibit a multivesicular appearance. Cargoes are concentrated in progressively fewer and larger endosomes that migrate from the cell periphery to the center, where they are carried to the late endosomes (Huotari and Helenius, 2011; Rink et al., 2005). Throughout the years there has been a debate as to whether cargo moves through vesicles between cell compartments of stable identity or if membranes enclosing cargo change their compositions through a maturation process (Griffiths and Gruenberg, 1991; Murphy, 1991). Early endosome functions depend on the existence of patches of short actin filaments onto the endosomal membranes (Muriel et al., 2017). F-actin plays an essential role in the biogenesis of MVBs and their transport beyond early endosomes, with the annexin A2 protein found in early endosomes, together with spire1, responsible for actin nucleation (Muriel et al., 2017). Moreover, branching activity is fundamental for these processes, with the Arp2/3 complex playing a key role. Two additional actin-binding proteins (ABPs), moesin and cortactin, were found to be necessary for the formation of F-actin networks that mediate endosome biogenesis, maturation, and transport through the degradative pathway (Muriel et al., 2016). Interfering with actin polymerization at any step of this process may prevent endosome maturation and thus transport of degradation-sorted cargo towards late endosomes and lysosomes (Muriel et al., 2017).

Bro1 is a cytoplasmic yeast protein that transiently associates with endosomes and that is required for the formation of intralumenal vesicles (Odorizzi et al., 2003). VipA was found to associate with this component of the MVB pathway, suggesting that the effector causes defects in the late steps of such pathway wherein fusion of endosomes with the vacuole occurs. Additionally, it colocalizes with early endosomes in infected macrophages, although neither the endocytic internalization nor the early endosome trafficking of cargo is affected by VipA. However, analysis in mammalian cells of VipA and the later components of the endosomal/MVB pathway LAMP-1, a marker of late endosomes, and Alix, a human homolog of Bro1, displayed low colocalization, indicating no interaction (Franco et al., 2012).

Assessment of colocalization between early endosomes and VipA variants revealed that $VipA_{\Delta NH2}$ displays significant lower colocalization with EEA1-labeled endosomes, as well as

$VipA_{NPY \rightarrow AAA}$, indicating that the N-terminal region is necessary for VipA interaction with early endosomes. Moreover, testing for the ability of all the previously mentioned variants to induce a Vps^- phenotype in yeast showed that $VipA_{\Delta CC}$ and $VipA_{\Delta Pro}$ were still able to cause a this phenotype, whereas all the others were unable to. Therefore, both N- and C-terminal regions are necessary to disrupt vacuolar trafficking in *S. cerevisiae* and, possibly, the Aspargine-Proline-Tyrosine (NPY) motif within the N-terminal region is also involved in this process (Bugalhão et al., 2016).

Vesicle coaters, adaptors, SNAREs, and Rab GTPases, have been found to act as key regulators of intracellular trafficking in eukaryotes. Rab GTPases mediate membrane tethering and act as endosomal membrane organizers since they regulate several host proteins, creating a mosaic of different membrane domains with different biochemical properties and functions (Barbero et al., 2002; Rothman and Söllner, 1997; Sönnichsen et al., 2000). These proteins constitute an important machinery which is peripherally associated with membranes, following a dynamic that is dependent on the equilibrium between guanine nucleotide exchange factors (GEFs) and GTPase activating proteins (GAPs). GEFs mediate the activation of Rab GTPases by promoting the exchange of bound GDP for GTP. GAPs, on the other hand, turn Rab GTPases off by stimulating their ability to hydrolyze GTP into GDP (Zhen and Stenmark, 2015). Different Rab domains were found to assemble and disassemble from endosomal membranes, and it has been postulated that such dynamics are central in endosome biogenesis and maintenance, as well as in cargo progression (Rink et al., 2005).

Recently, VipA was found to colocalize and interact with the small Rab5 GTPase. Moreover, this interaction was found to be independent of the C-terminal region of VipA, in which the actin-binding domain is located (Franco et al., unpublished). Rab5 is a key determinant of early endosomes, organizing host cell proteins into specific membrane subdomains. Cargo targeted for degradation is internalized into Rab5-containing endosomes and later appears in Rab7-containing endosomes, with Rab7 GTPase being a determinant of late endosomes. Work was done in order to understand if cargo is transferred from one entity to the other, or if endosomes lose Rab5 and acquire Rab7. A Rab conversion mechanism between Rab5 and Rab7 was identified within approximately 30 minutes of uptake of a labeled lipoprotein and found to be a crucial point in the differentiation between early and late endosomes. Moreover, Rab5-to-Rab7 conversion was found to coincide with endosomes movement away from cell periphery and endosome growth, and to be dependent on the ability of Rab5 to hydrolyze GTP. It was also found to require the class C VPS/HOPS complex, an established Rab7 GEF that was also found to interact with Rab5 (Rink et al., 2005).

In vitro work aimed to reconstitute actin nucleation and elongation on early endosomes by mixing cell-derived endosomal and cytosolic fractions. It revealed that stained actin filaments on Rab5-positive endosomes start to be visible at approximately 1 minute after the beginning of the reaction, and that actin structures rapidly become longer, branched, and linked to others, resulting in a complex actin network. Moreover, actin nucleation activity was found to be selectively associated with Rab5-postivie endosomes and not with other endosomes or cellular

membranes *in vivo*, which lead the authors to believe that actin nucleation activity is most likely associated with Rab5 endosomes. However, despite the identification of annexin A2 and spire as key determinants in actin nucleation, and of Arp2/3, moesin and cortactin as indispensable factors in F-actin branching and assembly, characterization of the components required for the formation of the actin network associated with early endosomes is still necessary for a better comprehension of this process (Muriel et al., 2017). The small Rab5 GTPase was also found to induce lamellipodia formation and cell migration, processes that depend on the reorganization of the actin cytoskeleton, suggesting a relationship between these processes and endocytosis (Spaargaren and Bos, 1999).

Since actin is involved in numerous trafficking processes, the finding of the direct VipA-actin interaction suggested that its ability to disrupt intracellular trafficking in yeast could be dependent on its interaction with actin. Colocalization between VipA and actin structures was observed in yeast, namely in the mother-bud neck in dividing cells, a site that contains the cytokinetic ring and is therefore enriched in actin filaments. Moreover, VipA appears as foci significantly colocalized with yeast ABPs. During macrophage infection, VipA colocalizes with both F-actin and early endosomes, with the most colocalization at 8 hours post-infection. Additionally, the VipA-1 mutant that is not able to cause a Vps^- phenotype in yeast, also displayed significant decrease in affinity for monomeric actin (Franco et al., 2012).

Yet, functional characterization of the different VipA regions presented evidence that VipA-mediated actin polymerization is essential but not sufficient for its ability to interfere with organelle trafficking in yeast, given that both mutants that bind and polymerize actin, and mutants that do not have this ability, were defective in inducing a Vps^- phenotype in yeast. Although the C-terminal region mediates VipA interaction with actin, the other regions are fundamental for its full action on filament growth, possibly modulating binding affinity and/or correctly positioning VipA during its interaction with actin (Bugalhão et al., 2016). The authors therefore hypothesized a model according to which both VipA binding to actin and localization to endosomes are needed to interfere with the eukaryotic vesicular trafficking. Moreover, they consider that this effector may be acting as a link between actin dynamics and the endocytic pathway, with the C-terminal region responsible for mediating the interaction with the actin cytoskeleton, and the N-terminal region responsible for the interaction with the endocytic vesicles.

1.6. Objectives

Infections by *Legionella pneumophila* remain a public health problem and there is still much to be done to combat this bacterium at both prevention and therapy levels. The *Legionella* VipA bacterial effector is translocated into the host cell during infection through a particular type of secretion system. VipA was found to enhance actin polymerization *in vitro* and to interfere with vesicle trafficking in yeast. Since organelle trafficking is an actin-dependent process, it has been hypothesized that the concerted action of VipA in these two processes may contribute to the formation of the specialized *Legionella*-containing vacuole in the *L. pneumophila* host cells.

In this work, a widefield fluorescence microscopy technique will be applied to *in vitro* assays in order to complement and extend on previous results from bulk assays regarding the role of VipA in enhancing actin polymerization, by introducing a visual component that allows the observation of individual fluorescent actin filaments. This aims to obtain new insight into how this effector enhances actin polymerization, and hopefully to clearly differentiate between its effects on nucleation and elongation. Moreover, for a better understanding of the potential effects of this protein *in vivo*, the same assays will be performed in the presence of profilin, a molecule that is typically found in complex with monomeric actin in eukaryotic cells. In addition, examination of the possible effects of the introduction of Rab5 GTPase in the *in vitro* VipA-mediated actin polymerization will be carried out, as this is an important eukaryotic marker of early endosomes and it was already found to bind VipA *in vitro* and to colocalize with VipA *in vivo*. Lastly, a protocol adapted from Rink et al., 2005, will be carried out for characterization of endosome maturation in fixed cells carrying a VipA-harboring vector, by means of confocal fluorescence microscopy. It will consist on the tracking of both Rab5 and a labeled endocytosed lipoprotein signals and further evaluation of colocalization between both components, in order to determine if it is maintained or lost over time, and therefore if VipA is interfering with Rab conversion.

2. Materials and methods

2.1. Overexpression and IMAC purification of His_6-VipA protein

Two or three colonies of *E. coli* BL21 (DE3) harboring a plasmid encoding His_6-VipA protein (pET15b-VipA) (Supplementary Table S2) were inoculated in 1 l of rich LB medium for auto-induction (LB (NZYTech), 1 mM $MgSO_4$, 1x 5052 solution, 1x NPS salts solution (Supplementary Table S1), and 100 µg/ml ampicillin (Sigma)) and left to grow at 37ºC with agitation for ~ 16 h. Cells were pelleted by centrifugation at 5,000 rpm for 20 min. The cell pellet was resuspended in 20 ml of Lysis Buffer (Supplementary Table S1). Cells were lysed by three passages in a French pressure cell press at 1,000 psi. PMSF (1 mM, AppliChem) was added every 15 min to the lysate which was kept on ice. The lysate was centrifuged twice at 10,000 rpm and 4ºC, for 30 min each time. An empty chromatography column (Bio-Rad) was packed with 1 ml of HisPur Ni-NTA superflow agarose (Thermo Scientific) and then equilibrated with 10 ml of Lysis Buffer. The supernatant of the lysed extract was loaded into the column which was afterwards washed twice with 10 ml of Wash Buffer (Supplementary Table S1). Finally, three different Elution Buffers with a gradient of imidazole concentration (100 mM, 200 mM and 500 mM) (Supplementary Table S1) were loaded in this order for five times each into the column, 1 ml each time. All fractions were kept and run in SDS-PAGE for confirmation. The final purified protein was dialyzed overnight in 1x PBS using a 7,000 kDa MWCO snakeskin membrane (Thermo Scientific). Afterwards, protein aliquots were run in SDS-PAGE along with BSA standards for concentration determination.

2.2. Wild type and constitutively active GST-Rab5 protein purification

Four ml of *E. coli* BL12 (DE3) carrying plasmids pIF415 or pIF416 (Supplementary Table S2) were both inoculated in 200 ml of LB medium supplemented with 0.1 mg/ml ampicillin (Sigma), and left to grow at 37ºC with agitation. At an OD_{600} ~ 0.5, 1 mM IPTG (NZYTech) was added and the cultures were left to incubate for 4 h at 37ºC with agitation. The total volume of each culture was centrifuged in Falcon tubes (previously cooled in ice) for 10 min at 5,000 rpm and 4ºC. After centrifugation, the supernatants were discarded, and the cell pellets were kept and stored at -20ºC overnight. The cell pellets were resuspended in 15 ml of cold 1x PBS and cells were then lysed by means of sonication (10 cycles of 1 min with 1 min intervals; 0.8 amplitude) and PMSF (1 mM) was added after the first cycle. The lysates were centrifuged twice for 20 min at 10,000 rpm and 4ºC, and later incubated for 1h at 4ºC in a rotating rocker with 1 ml of glutathione-sepharose slurry beads (GE Healthcare) previously washed 4 times with 5 ml of cold 1x PBS, at 800 x g for 2 min each time. Each mixture was loaded into a chromatography column (Bio-Rad) packed with glutathione-sepharose and washed three times with 10 ml of 1x PBS. Proteins were eluted five times with 1 ml of 1x PBS containing 10 mM of reduced glutathione (Sigma). All fractions were kept and run in SDS-PAGE for confirmation. Afterwards, proteins were dialyzed overnight in Storage Buffer (Supplementary Table S1) using a 7,000 kDa

MWCO snakeskin membrane for storage at -80ºC. Purified proteins were quantified by means of the Bradford Method.

2.3. SDS-PAGE with samples from protein purification

Gels were cast in two steps, starting with the preparation of a 12% (v/v) acrylamide (NZYTech) resolving gel, by mixing 400 mM Tris pH 8.8 buffer (Supplementary Table S1), 0.1% (v/v) SDS (NZYTech), 12% (v/v) acrylamide, 0.1% (v/v) APS (Carl Roth), 0.004% (v/v) TEMED (Amresco), and MiliQ water up to the desired volume. The mixture was applied into a vertical gel caster system (Bio-Rad) and left to polymerize. Water was added on top of the gel in order to smoothen the surface, prevent bubbles formation and accelerate polymerization. In a second step, a 5% (v/v) acrylamide concentration gel was prepared by mixing 125 mM Tris pH 6.8 buffer (Supplementary Table S1), 0.1% (v/v) SDS, 5% (v/v) acrylamide, 0.1% (v/v) APS, 0.1% (v/v) TEMED, and MiliQ water up to the desired volume, and adding 0.004% (v/v) Orange G (Scharlau) for a better visualization of the gel pockets formed after solidification and resulting from the insertion of a comb into the gel caster. Protein samples (15 µl/each) were mixed with 4 µl SDS loading buffer 5x (Supplementary Table S1) and boiled for 5 min at 100ºC. Samples were run along with 5 µl of LMW ladder (NZY Tech) at 100 V for approximately 2 h, using a Tris-glycine (1x) buffer (Supplementary Table S1) as electrolyte. Afterwards, gels were stained using a Coomassie Blue staining solution for ~ 30 min with agitation and further destained using a destaining solution (Supplementary Table S1) for ~ 1 h for a better visualization of the protein bands.

2.4. GST-Rab5 activation by GTPγS

In order to maximize permanent activation of GST-Rab5 molecules, loading with GTPγS, a non-hydrolysable form of GTP, was carried out. Protocol was adapted from Murray and Backer, 2005. The previously purified GST-Rab5 proteins were both incubated for 30 min at room temperature with 2 ml of Nucleotide Exchange Buffer (Supplementary Table S1) supplemented with 1 mM GTPγS (Jena Bioscience) in a 3 µM GST-Rab5 concentration. These solutions were then transferred to two Vivaspin® 6 ml Centrifugal Concentrator columns (MWCO 10 kDa) which were centrifuged twice at 4ºC and 5,000 g x for 2 min. Then, 2 ml of Nucleotide Stabilization Buffer (Supplementary Table S1) supplemented with 10 µM of GTPγS were loaded into each column, and both were centrifuged at 4ºC twice at 5,000 x g for 2 min and once at 2,000 x g for 2 min. The remaining ~ 200 µl of protein solution were then recovered and stored at -20ºC.

2.5. Actin polymerization *in vitro* assays

2.5.1. Flow cells preparation

Handmade flow cells were prepared as a sandwich of a glass slide (1.0 – 1.2 mm thick, Fisherbrand) with two Parafilm strips placed longitudinally over it with an approximately 15 mm wide channel between them and a glass coverslip (20 x 20 mm, Menzel-Gläser) on top (Figure 1). This set was heated at 100ºC until Parafilm melted so the system became stuck and assembled. Liquid was introduced using a micropipette on one side of the chamber concomitantly using an absorptive cloth on the other side to pull it through the flow cell. Before sample introduction, the flow cells were incubated with 50 µl of 10% (w/v) BSA (Fisher Scientific) for 10 min to avoid adsorption of actin to the surfaces of the glass. Flow cells were washed with 90 µl of G-buffer (Supplementary Table S1) and then 20 µl of filamin (0.1 mg/ml) (filamin from turkey smooth muscle, Hypermol) was applied as tethering protein and left to incubate for 5 minutes. Finally, flow cells were washed again with 90 µl of G-buffer.

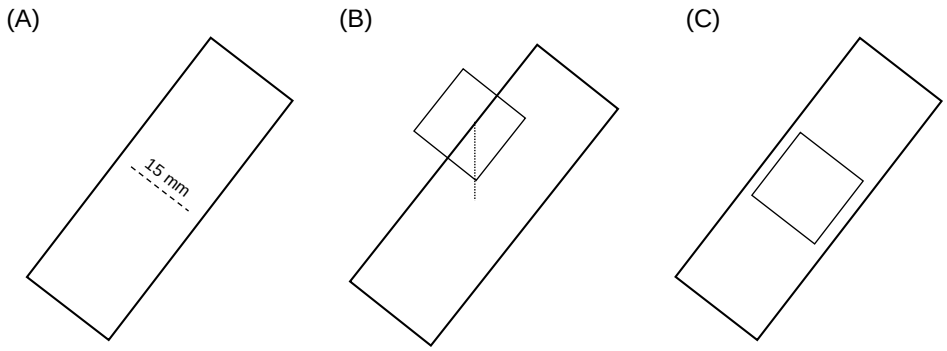

Figure 1. Scheme of handmade flow cells preparation. (A) Two Parafilm strips are placed longitudinally over a glass slide with a 15 mm wide channel in between. (B) A glass coverslip is placed on top of the parafilm slices. (C) The system is heated until Parafilm melts to assemble the system.

2.5.2. Actin polymerization in the presence of VipA

Each sample was prepared in a total volume of 100 µl. First, 100 nM Atto488-Actin (α-skeletal muscle actin from rabbit skeletal muscle, Hypermol) was incubated for 5 minutes in ice with G-buffer and 5% (v/v) of 10x ME buffer (Supplementary Table S1) for Ca^{2+} to Mg^{2+} exchange. His_6-VipA was added to the solution after such incubation for a concentration of 10, 25, 50 or 100 nM. For negative control purposes, 1x PBS buffer was used instead of His_6-VipA solution. This mixture contained 50% (v/v) of the sample final volume, adding G-buffer up to the desired volume. Upon incubation, the actin-containing solution was immediately mixed with 10% (v/v) of 10x KMEI and 40% (v/v) of imaging buffer (Supplementary Table S1). The total volume of sample was introduced into the flow cell as above mentioned and both open laterals of the coverslip were sealed with grease (korasilon-paste, GmbH) to prevent sample from drying.

2.5.3. Actin polymerization in the presence of VipA and profilin

To determine whether the addition of profilin had an impact on VipA-mediated actin polymerization *in vitro*, samples were prepared according to 2.5.2, with 0.7 µM profilin (Profilin1, Human recombinant, Hypermol) added to the initial actin-containing solution prior to incubation.

2.5.4. Actin polymerization in the presence of VipA and Rab5

To assess whether GST-Rab5 influences VipA-mediated actin polymerization *in vitro*, samples were prepared according to 2.5.2, with His_6-VipA and 0.1 µM GST-Rab5 (in the GST-Rab5:GTPγS form) prior to incubation on ice for 20 min. The same assays were performed for both wild-type GST-Rab5 and a constitutively active mutant (GST-$Rab5^{CA}$, carrying amino acid substitution Q79L).

2.5.5. Microscopy and image acquisition

Widefield imaging was done on a Leica DMI6000 inverted microscope, using illumination from a Leica EL6000 source ensuring minimal photobleaching during acquisition, and using a fluorescence filter cube with the Leica GFP ET filter set, a 100x/1.46 a-plan apochromat oil immersion objective plus a 1.6x magnifier, Leica type F immersion oil, and an Evolve 512 electron microscopy charge-coupled device (EM-CCD) camera (Photometrics) using 16-bit EM gain amplification. The final pixel size was 100 nm. Metamorph software (version 7.8.4.0) was used to control the imaging process, and the defined multi-dimension acquisition settings were gain (1x); EM gain (200); exposure time (200 ms) and digitizer (5 MHz). For assessment of actin polymerization over time, one-hour time-lapse videos were obtained starting five minutes after sample preparation, acquiring one image every 1 min. To evaluate nucleation at early time points with higher number of images, at least 20 images of different fields of view were acquired for every sample approximately five minutes after sample preparation.

2.5.6. Image processing and analysis

Imaging analysis started with modification of recently reported software for automated cell segmentation, tracking, and lineage reconstruction, DeLTA, which was used to train neural networks to segment and track growing *E. coli* cells (Lugagne et al., 2019). DeLTA uses separate U-nets for segmenting and tracking. The U-net is a convolutional network architecture developed for fast and precise segmentation of biomedical images (Ronneberger et al., 2015). A set of 20 images representative of the variety of filament density were chosen to generate the training data set. The 20 images were initially rescaled to a range of 1,000 to 10,000 EMCCD counts, and then blurred by applying a 1-pixel Gaussian blur filter using ImageJ software (version 1.52p) (Figure 2C). The same transformations were applied to the data later segmented using the U-net. The Ridge Detection ImageJ plug-in (version 1.4.0) was used to semi automatically detect filaments after manually optimizing parameters for each individual

image (Figure 2D), and then all the images were transformed into black and white binary images by binary dilation of the single-pixel-width ridges (Figure 2E) and converted to weight images based on the number of filament and non-filament pixels (Figure 2F). Because of the low number of training images and the over 30 million trainable U-net parameters, the training data was augmented to avoid overfitting and increase the diversity of training data. Training data was augmented by defining five different DeLTA parameters: rotation (0.5); shiftX (0.5); shiftY (0.5); zoom (0.15); and horizontal flip (true). Image blurring described above was necessary because fluorescent images were noisy and most of the augmentation operations interpolate pixels, introducing blur. In initial attempts without blurring all data, the augmented training set had less pixel noise than the data to be segmented and segmentation performance was poor.

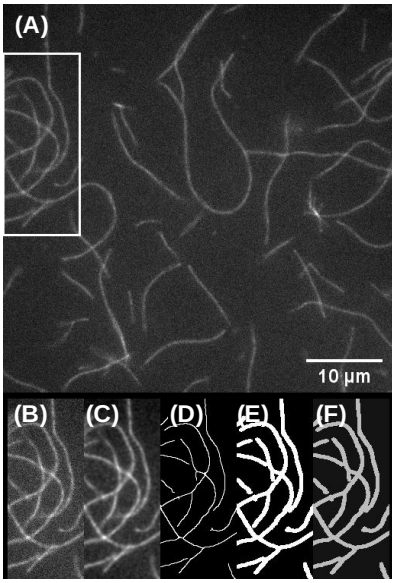

Figure 2. Steps for generation of the training data set. A set of 20 images representative of the variety of filaments density were chosen to integrate the training data set. The original images (A and B) were first modified by the application of a blur filter (C). The Ridge Detection plug-in of ImageJ was used to correctly detect the filaments by manually optimizing the parameters to each individual image, and then a black and white binary image was created (D). Afterwards, images were modified again by using a filter to dilate the filaments (E). Binary segmented images were converted to weight images based on the number of filament and non-filament pixels (F).

The performance of the U-net was optimized by minimizing loss of the weighted binary cross entropy function for single, randomly selected and randomly augmented images. The Adam optimizer was used with a learning rate of 1e-4. Weights were calculated by summing the number of filament and non-filament pixels in the 20 training segmentation images, and weighted such that filament and non-filament pixels had equal overall influence on training (because there are more non-filament pixels in training data, training the network without weighting would lead to a bias towards predicting non-filament pixels). Training was carried out in 250 epochs of 250 steps each (1 image per step; a limitation for the 512x512 pixel images given the size of the U-net and limitations on memory), with the U-net model weights saved and

performance evaluated after each epoch. In addition to blurring data for training and segmentation, we found that a key parameter was the extent of dilation of the single-pixel filaments after ridge detection (Figure 2E), with it being difficult to train a network capable of segmenting very thin filaments. A complete training run took several hours on a GeForce 1050TI GPU with 4 gigabytes of memory; once trained, the network could segment individual images in ~ 100 ms.

After improving the model through cycles of training and testing on a subset of experimental data, all images were segmented by the trained U-net. The output was then subjected to automated detection of the filaments using Ridge Detection ImageJ plug-in with the same parameters for all images. Output of analysis with Ridge Detection provided data for both number of filaments and their respective lengths. Representative images of image segmentation after training the model and filaments detection using Ridge Detection plug-in are presented in Figure 3. Comparative quantitative analysis was done through custom Python scripts using JupiterLab (version 1.0.2). Data was compiled into Pandas data frames, processed using NumPy functions, and plotted using Seaborn and Matplotlib.

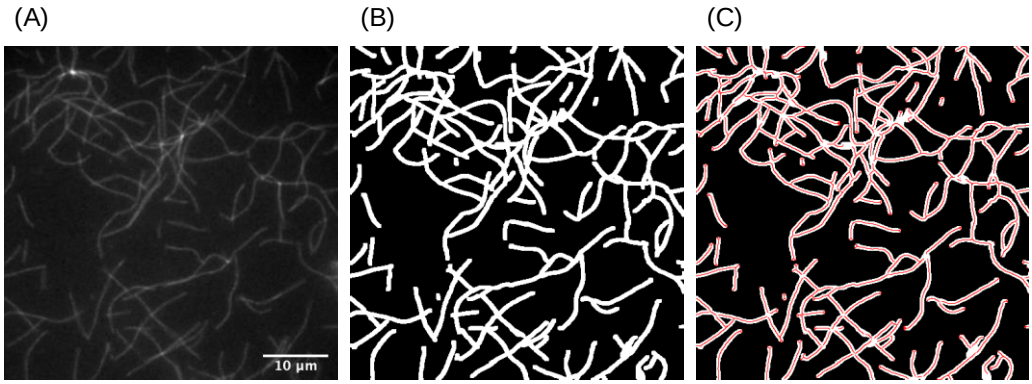

Figure 3. Result of filament segmentation using the U-net network and detection using the ImageJ Ridge Detection plug-in with the established parameters. (A) Representative image of the raw data introduced into the trained network for segmentation. (B) The same image after segmentation by the trained U-net. (C) Filament detection by the Ridge Detection plug in of ImageJ.

2.6. DiI-LDL pulse-chase experiment in HeLa GFP-Rab5c\ cells

In order to assess whether VipA impairs endosome maturation by interfering with Rab5 to Rab7 conversion, an experiment adapted from previous work of Rink et al., 2005, was carried out, consisting in the tracking of colocalization between fluorescent Rab5 and an internalized fluorescent lipoprotein over time, to determine whether such colocalization was maintained or lost, and therefore if Rab conversion was taking place.

2.6.1. Cell growth and maintenance

A HeLa Kyoto cell line stably expressing near endogenous levels of GFP-Rab5c was kindly provided by Marino Zerial's group (Max-Planck Institute of Molecular Cell Biology and Genetics, Dresden, Germany). In order to generate this cell line, the authors used a bacterial artificial chromosome (BAC) to tag Rab5c, the most abundant Rab isoform in HeLa cells, with GFP (Franke et al., 2019). Cells were grown in disposable 100 mm dishes (Thermo Scientific), in DMEM (1x, Gibco) supplemented with 10% (v/v) FBS (Gibco), 1% (v/v) glutamine (Gibco), 1% (v/v) pen/strep antibiotic (Gibco), and 400 µg/ml of geneticin disulphate (G418) solution (Carl Roth) for selection. Cells were maintained at 37ºC in controlled humidified atmosphere with 5% CO_2, with weekly passages by means of the trypsinization method (TrypLE express dissociation reagent, Gibco).

2.6.2. Cell seeding

Cell seeding was carried out in 15 µ-slide 8-well glass bottom plates (Ibidi) after passaging, previously counting the number of cells using a Neubauer chamber for an approximate amount of 15,000 cells per well. Cells were seeded in 250 µl of complete growth medium per well. Four plates were used, each one corresponding to one time-point after the end of Dil-LDL pulse (2.6.5). Cells were incubated at 37ºC and 5% CO_2 for ~ 20 h.

2.6.3. Cell transfection

Six wells were used in each plate, half of them for transfection with the *vipA*-harboring plasmid (pIF328) (Supplementary Table S2) and the other half for transfection with the original transfection vector (pEF6/Myc-His A) (Supplementary Figure S2). Transfection was carried out by mixing in both cases 200 µl of jetPRIME® buffer, 2 µg of DNA, and a 1:3 DNA to jetPRIME® reagent ratio (Polyplus transfection), and by adding 6.5 µl of the solution in each of the corresponding medium-containing wells. Cells were then left to incubate at 37ºC and 5% CO_2 for ~ 24 h.

2.6.4. Serum starvation

Complete growth medium was aspirated, and cells were washed once with 1x PBS pH 7.4 (Gibco). Immediately after, 250 µl of serum deficient DMEM (0.2% (v/v) FBS) was added to each well and cells were left to incubate at 37ºC and 5% CO_2 overnight.

2.6.5. Dil-LDL pulse

After cell serum starvation, the medium was aspirated and replaced by Dil-LDL (Alfa Aesar) containing medium (5 µg/ml of Dil-LDL in 0.2% (v/v) FBS-containing DMEM, previously vortexed). A 10 min pulse was carried out at 37ºC and 5% CO_2. Next, the medium was

aspirated and replaced by serum-deficient DMEM lacking Dil-LDL. Thereafter, cells were left to incubate again at 37ºC and 5% CO_2 and fixed at the corresponding time-point after Dil-LDL pulse (0, 10, 20 and 40 min after Dil-LDL pulse).

2.6.6. Cell fixation and immunostaining

For cell fixation at the corresponding time-points, cells were first washed with 250 µl 1x PBS and incubated in 3% paraformaldehyde (Alfa Aesar) for 20 min with light agitation. Cells were then washed three times with DPBS (Lonza) with agitation, for 5 min each wash. Permeabilization took place by incubating the samples with 0.1% (v/v) Triton X-100 (Fisher Chemical) in PBS for 10 min with agitation, followed by three 10 min washes with DPBS. To block possible antibody unspecific binding, cells were incubated with 250 µl of 1% (w/v) BSA in 0.1% (v/v) Triton X-100 for 1 h with agitation. Afterwards, cells were incubated overnight with a Mouse anti-c-Myc primary antibody (Calbiochem), previously diluted 1:500 in 1% (w/v) BSA. The solution was decanted, and cells were then washed three times with DPBS with agitation, 5 min each wash. Lastly, incubation with 1:500 diluted Alexa Fluor®647-conjugated Donkey anti-Mouse secondary antibody (Jackson ImmunoResearch) took place for 2 h with agitation in the dark, and cells were ultimately washed three times with DPBS for 5 min with agitation, keeping them at 4ºC in DPBS in the dark after the last wash.

2.6.7. Microscopy and image acquisition

Imaging was performed in a Zeiss LSM 880 with Airyscan confocal light microscopy, using fluorescence (HCP UV lamp) to locate cells for confocal imaging, a 63x Plan-Apochromat 1.4NA oil immersion objective (Zeiss), Immersol™ (Zeiss), and the 488, 561 and 633 nm laser lines, for GFP-Rab5, Dil-LDL and Alexa 647-VipA imaging, respectively. Two different photo-multiplier tube (PMT) detectors were used for both GFP (Rab5) and Alexa 647 (VipA), and a Gallium Arsenide Phosphide (GaAsP) detector was used for Dil-LDL imaging. Emission wavelength ranges were adjusted manually to maximize collected light and minimize background and crosstalk. Confocal Z-series stacks (600 nm interval between planes) were acquired beginning by manually finding the approximate bottom and top of the cells to define as first and last planes. Settings used for 488 nm laser line were: power (5% of maximum power); pinhole (50.5); Gain (700). For 561 nm laser line, power (10.0), pinhole (56.9) and Gain (500). In the case of the 633-laser line, power (5.0), pinhole (56.9) and Gain (700). For all laser lines, digital gain was 1.0. The Zeiss Zen 2.3. (black edition) software was used to control the microscope. Each plan was scanned with a resolution of 66 nm each with a 1 µs dwell time.

2.6.8. Image processing and analysis

Images were first processed in Fiji (ImageJ-win64) using the segmentation tool to outline individual cells and then setting pixels outside of the cell boundary to zero in all channels. Using

ImageJ plug-in JACoP (Bolte and Cordelières, 2006), a threshold for pixel intensity was established for all the three channels used based on one image with relatively good signal for each, in order to exclude the background (autofluorescence, detector noise, and nonspecific binding for immunostaining). Quantitative analysis of co-localization was performed by calculating the Manders' coefficients as described by the authors, which correspond to the fraction of pixels of one channel that overlap the pixels of other channel in relation to the total pixels of the first one. The Manders' coefficients were calculated automatically for all the images by means of Python a script written and executed in JupiterLab (version 1.0.2), which contained a function for splitting the image into the three different channels, and then applied a function corresponding to the previously described for calculation of the Manders' coefficient in maximum intensity, Z-projection images, using the previously determined thresholds. The number of cells imaged per condition was n>11.

2.6.9. Preliminary experiments in live cells

In order to first visualize the internalization of DiI-LDL by the cells mentioned above, preliminary experiments lacking transfection with the VipA-containing vector were carried out in live cells. The same HeLa cell line stably expressing near endogenous levels of GFP-Rab5c was seeded and serum starved following the previously described procedure (2.6.2 and 2.6.4). After serum starvation, the medium was aspirated and replaced by serum deficient (0.2% (v/v) FBS) Leibovitz's L-15 medium (Gibco) and cells were taken to the microscope (previously heated) and remained ~ 1 h inside the microscope at 37ºC before imaging. A 15-min pulse of DiI-LDL was applied by aspirating the medium inside the plates with a micropipette and replacing it by 250 µl of Leibovitz's L-15 medium containing 10 µg/ml of DiI-LDL, previously vortexed. Next, medium was replaced again by DiI-LDL-free Leibovitz's L-15 medium. Alternatively, 10 µg/ml of DiI-LDL were directly applied to the medium and continuous uptake of DiI-LDL was imaged. Imaging was carried out using a Leica DMI6000 inverted microscope, illumination from a Leica EL6000 source at maximum intensity, a fluorescent filter cube Leica GFP ET filter set and an RFP fluorescence filter cube (custom filter set with Semrock filters FF01-561/13, FF02-616/73, and DI02-R561), a 100x/1.46 a-plan apochromat oil immersion objective plus a 1.6x magnifier, Leica type F immersion oil, and an Evolve 512 electron microscopy charge-coupled device (EM-CCD) camera (Photometrics) using 16-bit EM gain amplification. Final pixel size was 100 nm. Exposure time used was 25 ms. Metamorph software (version 7.8.4.0) was used to control the imaging process.

3. Results

3.1. Purification of His_6-VipA and GST-Rab5 proteins

Protein purification through affinity chromatography using the poly-histidine (His_6) and the glutathione S-transferase (GST) tags was successful for both VipA and Rab5 (wild type and mutant) proteins. His_6-tag fused proteins bind to Ni-NTA in IMAC affinity chromatography columns. VipA has a molecular weight of 39.6 kDa (EMBL-EBI, 2004) and His-tags have a relatively small size (~ 2.5 kDa), which is in accordance with the ~ 40 kDa band corresponding to the fractions after elution with 200 mM of imidazole observed after running samples from His_6-VipA purification in SDS-PAGE (Figure 4). A pool of the fractions corresponding to elution with 200 mM imidazole was used in subsequent experiments.

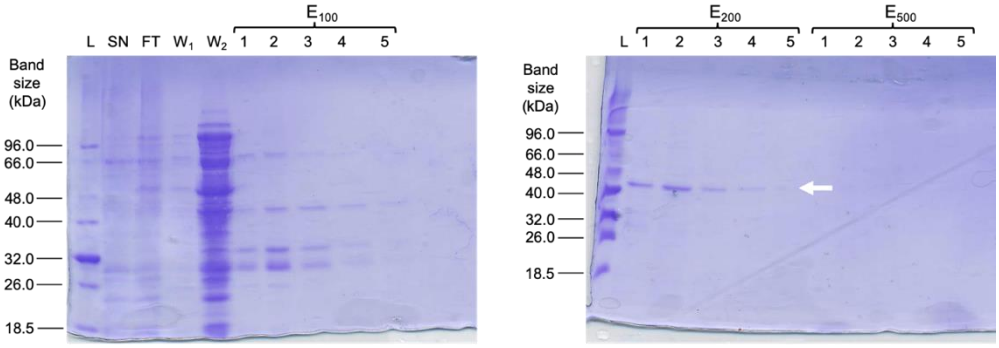

Figure 4. SDS-PAGE with samples from His_6-VipA purification. Fractions: L – ladder; SN – supernatant; FT – flow through; W_{1-3} – washes; E_{100} – elution fractions with 100 mM imidazole; E_{200} – elution fractions with 200 mM imidazole; and E_{500} – elution fractions with 500 mM imidazole.

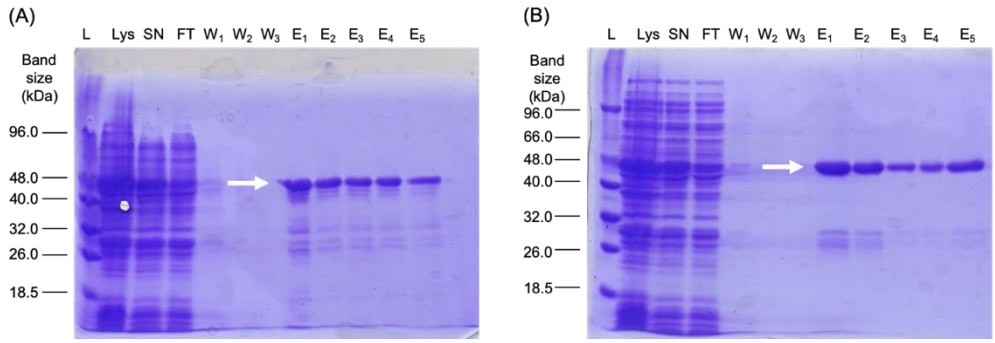

Figure 5. SDS-PAGE with samples from GST-Rab5 purification. (A) Wild-type GST-Rab5. (B) Constitutively active mutant. Fractions: L – ladder; Lys – lysate; SN – supernatant; FT – flow through; W_{1-3} – washes; and E_{1-5} – elution fractions with 10 mM of reduced glutathione.

Following the same rationale, the GST-tag, with a molecular size of 26 kDa, binds to reduced glutathione chromatography columns (Kimple et al., 2013). Rab5 GTPases are molecules of 22–24 kDa (EMBL-EBI, 1996). This matches the ~ 48 kDa band corresponding to

the elution fractions of wild type and constitutively active GST-Rab5 (Figure 5). All the elution fractions of both GST-Rab5 variants were used in further experiments.

3.2. Evaluation of F-actin density by real-time visualization of actin polymerization *in vitro*

Time-lapse videos were performed in order to visualize growth of the actin filaments over time in the absence or presence of His_6-VipA, and to determine whether profilin or activated GST-Rab5 molecules had an impact on such growth. The number and length of filaments were estimated using the ImageJ Ridge Detection plug-in, and the total length of all the filaments was the best metric to compare images at different time-points and conditions with a wide variation of filament densities. At high densities with many overlapping filaments, Ridge Detection analysis does not correspond perfectly to the actual numbers and lengths of filaments. Filament tracing is ambiguous at points where filaments overlap, leading to an overestimation of the number of filaments and an underestimation of average filament length at high densities. Therefore, total filament length was used for analysis, which corresponds to the extent of actin polymerization.

There was high variability among independent replication experiments, hindering the analysis process. The variability was mostly often characterized by conditions that usually showed robust polymerization but showed little or no polymerization in, at most, 1 of 3 independent replicates. We hypothesized that the variation stemmed from intrinsic limitations of the experimental protocol rather than from an actual biological variability. For instance, an imperfect sealing of the sample can result in sample drying and consequent change in component concentrations. Air bubbles were often observed in the sample chamber at different levels in different replicates. In some replicates, filaments stuck poorly to the glass surface, indicating variability in filamin coating of the coverglass. The observation of occasional replicates with little or no polymerization is in disagreement with previous data from bulk assays (Franco et al., 2012). Careful analysis of the results through the three independent replicates, as well as the awareness for the underlying downsides of the system, motivated the establishment of a rule to exclude from further analysis data considered to artifactually fail to exhibit polymerization. Hence, curves in which the total filament length value by the end of one hour of experiment does not reach at least 50% of the highest value verified for the same condition in a different replicate, were considered outliers and consequently excluded. Data curves excluded from analysis are presented in Supplementary Figure S1.

3.2.1. VipA enhanced actin filaments formation

The same VipA concentrations that displayed a trend in the effect of VipA-mediated actin nucleation in previous bulk assays (Franco et al., 2012) were used in these experiments. Yet, actin concentration required an adjustment since higher concentrations led to nearly complete polymerization after 5 minutes in the presence of the higher VipA concentrations. The chosen

100 nM actin concentration proved to be ideal since it allowed visualization of few small filaments in the absence of VipA at the initial time-point, necessary to correctly focus the sample, as well as of several longer yet individual filaments in the presence of 100 nM of the bacterial effector.

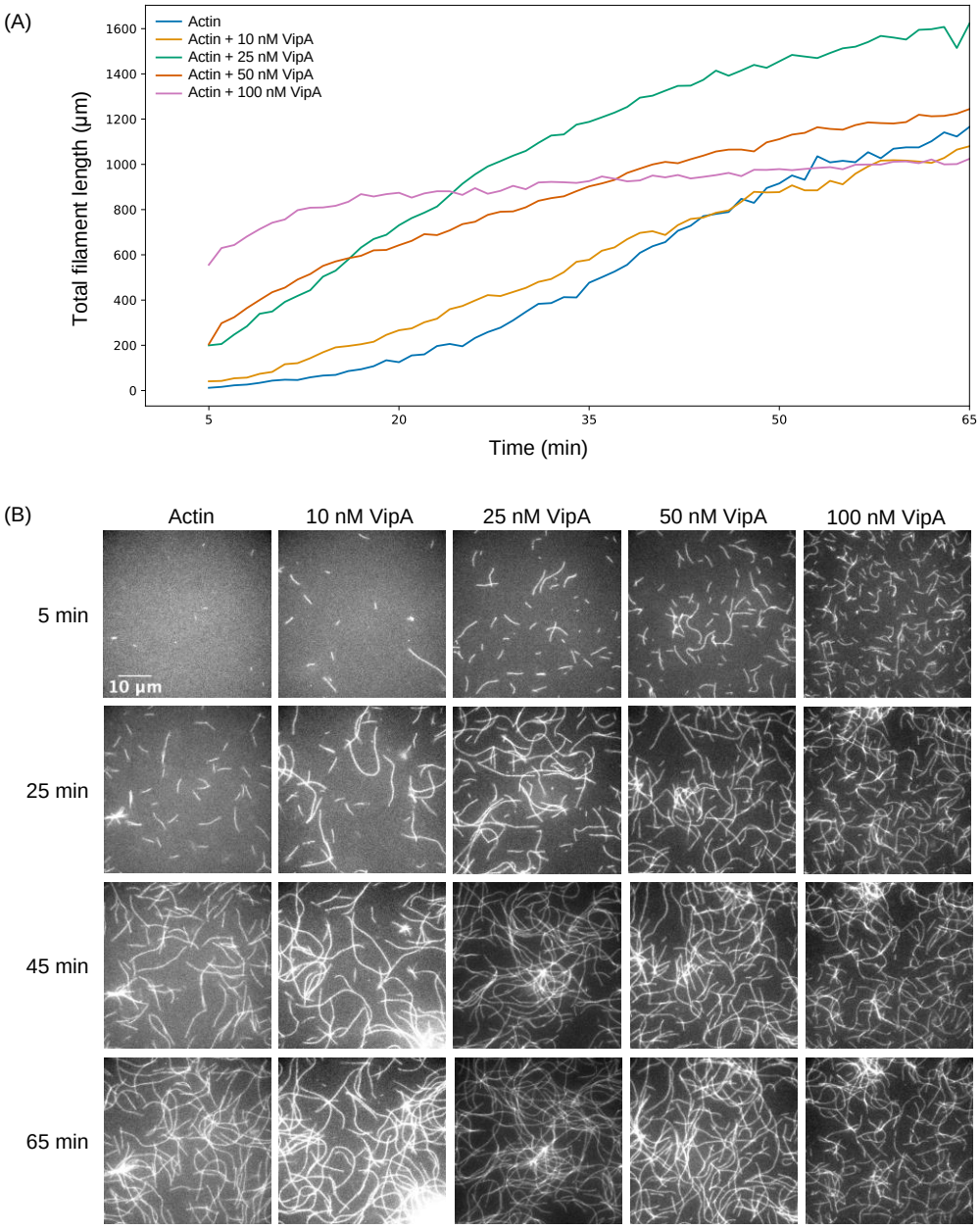

Figure 6. Actin polymerization over time in the presence of VipA. Samples contained 100 nM of Atto 488-monomeric actin and the displayed VipA concentrations. (A) Total filament length over time in the presence of different VipA concentrations, excluding data considered as outlier. Data is an average of n=2–3. (B) Representative images of actin polymerization over time in the presence of different VipA concentrations. For each condition, the same field of view was imaged for 1 h starting at 5 min after sample preparation.

As anticipated, the addition of VipA increased actin polymerization *in vitro* in a concentration-dependent manner when total filament length is observed after 5 minutes, as depicted in Figure 6A. Moreover, in the presence of 100 nM of VipA, the total filament length is stabilized at approximately 15 minutes of reaction. Then, a plateau is reached at which point growth stops, either because assembly is balanced by disassembly or because no more monomers are available. Despite the existence of a continuous increase in the total filament length in the presence of 25 nM of VipA, most likely due to technical-linked variability, all the curves reach similar values by the end of 1 hour of experiment, with such values being achieved faster in the presence of 50 or 100 nM of VipA. These results reproduce fairly well previous results from pyrene-actin assays that measured total actin polymerization fluorescence signal, except for the condition containing 25 nM of the bacterial effector (Franco et al., 2012).

Given the previously described role of VipA as an actin nucleator, these results can be linked to a higher initial number of filaments formed in the presence of VipA in a concentration-dependent manner. These filaments achieve their maximum growth faster probably because G-actin is consumed more rapidly in *de novo* filament formation. However, these results do not exclude a possible role of VipA in increasing the rate of addition of actin monomers to the filaments as well.

Observation of qualitative data (Figure 6B) indicates that differences in the total filament length after 5 minutes are indeed due to a higher number of filaments formed in the presence of increasing VipA concentrations rather than in spontaneous actin polymerization. In the presence of 10 nM of VipA, however, the major difference is linked to the average length of the initially formed filaments, rather than to a higher number, when comparing to the actin-alone sample. This suggests that although this VipA concentration is not sufficient to remarkably increase the number of nucleation events, it is sufficient to accelerate the process.

The presumable higher number of initially formed filaments (Figure 6A and Figure 6B) and the faster length stabilization (Figure 6A) corroborate a role for VipA in enhancing the nucleation step, leading to a higher number of actin polymerization “seeds” in less time.

3.2.2. Profilin interfered with actin polymerization and VipA-mediated nucleation

Previous results from pyrene-actin assays (Franco et al., 2012) and time-lapse videos of actin polymerization over time shown in this work are strong evidence that VipA acts as an actin nucleator *in vitro*. However, its behavior *in vivo* may not be identical because host cell components may modulate and limit VipA’s nucleation activity. The capacity to nucleate actin in complex with profilin is a *conditio sine qua non* for VipA to function as a strong actin nucleator in the *Legionella* hosts, since this is believed to be the most common form of ATP-bound monomeric actin in eukaryotic cells. Thus, time-lapse experiments were performed in the presence of a concentration of profilin seven times higher than the actin concentration, in order to ensure the formation of profilin-actin complex units without promoting excessive dynamic instability of filaments (Pernier et al., 2016). Experiments with both the highest and lowest

previously used VipA concentrations were repeated in the presence of profilin in order to assess whether the observed concentration-dependent effects of VipA on actin nucleation were maintained.

In both absence and presence of 10 nM VipA, total filament length at 5 minutes is not affected by the presence of profilin, as evidenced by Figure 7. Over time, differences start to appear, and total filament length after 1 hour presents lower values for both conditions in the presence of profilin, with approximately 100 and 300 µm difference, respectively. This suggests that the addition of profilin has an effect on actin polymerization, which is consistent with a role of this protein in sequestering ATP-actin monomers and in enhancing filament disassembly. In the presence of 100 nM of VipA, a ~ 200 µm decrease in the total filament length is observed at 5 minutes and slightly decreases over time, suggesting that profilin in solution decreases VipA's activity on actin nucleation, which can be explained by a G-actin sequestering by profilin that results in a difficulty of VipA to bind and recruit monomers for nucleation. Yet, the observed concentration-dependent nucleation activity of VipA indicates that it is able to enhance actin nucleation *in vitro* in the presence of profilin.

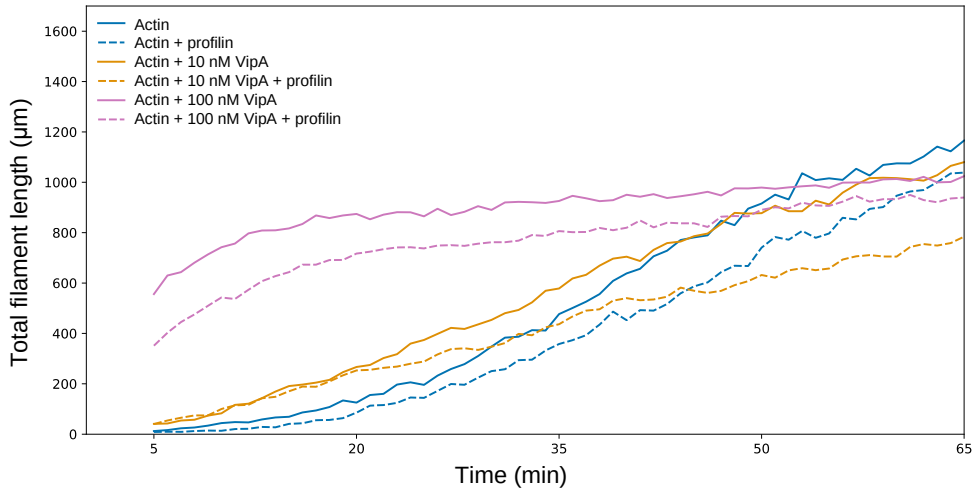

Figure 7. Actin polymerization over time in the presence of profilin. Samples contained 100 nM of Atto 488-monomeric actin, 700 nM of profilin1 (human recombinant), and the displayed VipA concentrations. Data considered as outlier were excluded from analysis. Data is an average of n=2–3.

3.2.3. Active Rab5 GTPases affected actin polymerization and delayed VipA-mediated nucleation

Given preliminary results from co-immunoprecipitation, colocalization and bacterial two-hybrid assays, which indicate that VipA interacts with the Rab5 GTPase (Franco et al., unpublished), experiments for visualization of actin polymerization in real-time were carried out in order to assess whether Rab5 influences actin polymerization and VipA-mediated actin nucleation *in vitro*. Wild-type and constitutively active Rab5 variants were used in these assays,

previously loaded with GTPγS, a non-hydrolysable form of GTP (Barbieri et al., 1994). The constitutively active mutant carries the amino acid substitution Q79L and is known to be defective in GTP hydrolysis. Loading with GTPγS increases activation of Rab5, which is active in the GTP:Rab5 form (Zhen and Stenmark, 2015), and allows to determine whether a process is dependent on GTP hydrolysis. Thus, all experiments were carried out in conditions of high Rab5 activity by using a non-hydrolysable GTP analog or a constitutively active mutant, and analysis of the effects caused by both active Rab5 forms was aimed at evaluating the efficiency of the activation procedure. A 1:1 actin-Rab5 ratio was used for a better characterization of the effects of the active GTPases on actin *in vitro*. The 100 nM VipA concentration that previously displayed a strong effect on actin nucleation was used to assess whether this effect was impaired by the presence of Rab5 molecules in solution.

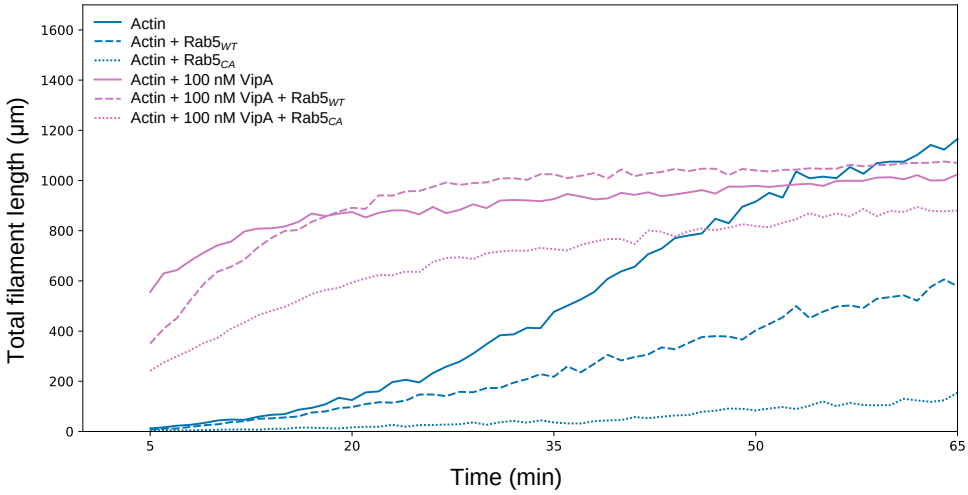

Figure 8. Actin polymerization over time in the presence of activated wild type or constitutively active Rab5. Samples contained 100 nM of Atto 488-monomeric actin, 100 nM of Rab5 (wild type or constitutively active mutant), and the displayed VipA concentrations. Data considered as outlier were excluded from analysis. Data is an average of n=2–3.

In the absence of VipA, no differences were observed in the total filament length at 5 minutes between conditions with no Rab5 and with either of the Rab5 variants, as shown in Figure 8. From this time-point, a decrease in the total filament length is observed for both types of Rab5, with the constitutively active mutant displaying a higher effect. After 1 hour, $Rab5_{WT}$ and Rab_{CA} present a decrease of total filament length relative to the condition with spontaneous actin polymerization of 600 and more than 1,000 µm, respectively, indicating that activated Rab5 molecules are interfering with actin polymerization. In the presence of 100 nM VipA, total filament length at 5 minutes is higher for both Rab5-containing conditions with respect to conditions lacking VipA, although lower (less ~ 200 and ~ 400 µm, respectively) than when compared to conditions with no Rab5. These results are consistent with a role for Rab5 in binding to G-actin, avoiding both spontaneous polymerization and nucleation by VipA. However, after 1 hour, differences between VipA-containing solutions are reduced.

The higher effect in inhibiting actin polymerization displayed by the constitutively active variant seems to indicate that $Rab5_{WT}$ is not permanently activated by binding to GTPγS. Furthermore, the differences observed in the total filament length after 1 hour in the absence of VipA, in contrast to the more similar values between conditions in the presence of VipA, suggest that either the overall number of filaments throughout the experiment or their respective lengths is higher in the presence of VipA.

3.2.4. Fitting of total filament length into a logistic model and estimation of half-time (τ), maximum total filament length (*m*), and growth rate (*k*) parameters

The obtained total filament length curves were fitted using a least squares regression into a logistic growth model defined by the function:

$$y = \frac{1}{1 + e^{-x}}$$

In the logistic growth model, unlike what occurs in the exponential growth model, growth is limited as resources are exhausted, eventually reaching a plateau level that represents the maximum supported size, *m*, known as carrying capacity when referring to modelling of populations (Weisstein, 2019). In this case, *m* corresponds to the maximum of total filament length and is related to the total polymerization after one hour. At this point, filament growth reached a plateau in all experimental conditions, consistent with a depletion of available monomeric actin. A time parameter, τ, is the time at which half of the *m* filaments are formed and is inversely proportional to the nucleation rate, with a lower τ indicating a faster nucleation rate. A rate parameter, *k*, is proportional to the rate of growth after nucleation and is therefore equivalent to the elongation rate, with a maximum value at $\frac{k\,m}{4}$. A representative plot of the logistic fit for the curves obtained from quantitative analysis of time-lapse data is shown in Supplementary Figure S2. The resulting function characterized by the above-mentioned parameters is the following:

$$f(x) = \frac{m}{1 + e^{-k(x-\tau)}}$$

In the absence of other proteins, VipA displayed a higher nucleation rate, with τ corresponding to less than 5 minutes, in the presence of 100 nM of VipA, whereas in the absence of VipA or with a 10-fold lower VipA concentration, τ was approximately 35 minutes (Figure 9A). Intermediate VipA concentrations exhibited faster nucleation when compared to spontaneous actin polymerization, with a τ of approximately 25 minutes. Moreover, no systematic differences in either *m* or *k* parameters were observed with increasing VipA concentrations, supporting that this bacterial effector acts mainly at the nucleation step of actin polymerization.

Figure 9B displays small, difficult to compare, differences between conditions with and without profilin in both absence and presence of VipA. In general, except in the presence of 10

nM of VipA, the addition of profilin slightly increased τ and decreased both *m* and *k*, on average. However, for individual replicates the experimental variability is greater than the change in any one parameter and individual comparisons are impossible with small sample sizes (n=2–3). The results were, on the whole, consistent with a role of profilin in sequestering monomeric actin. Sequestering actin monomers could reduce the rates of nucleation and/or elongation. Nevertheless, these results sustain that VipA, even at a low concentration, is able to nucleate actin *in vitro* in the presence of profilin.

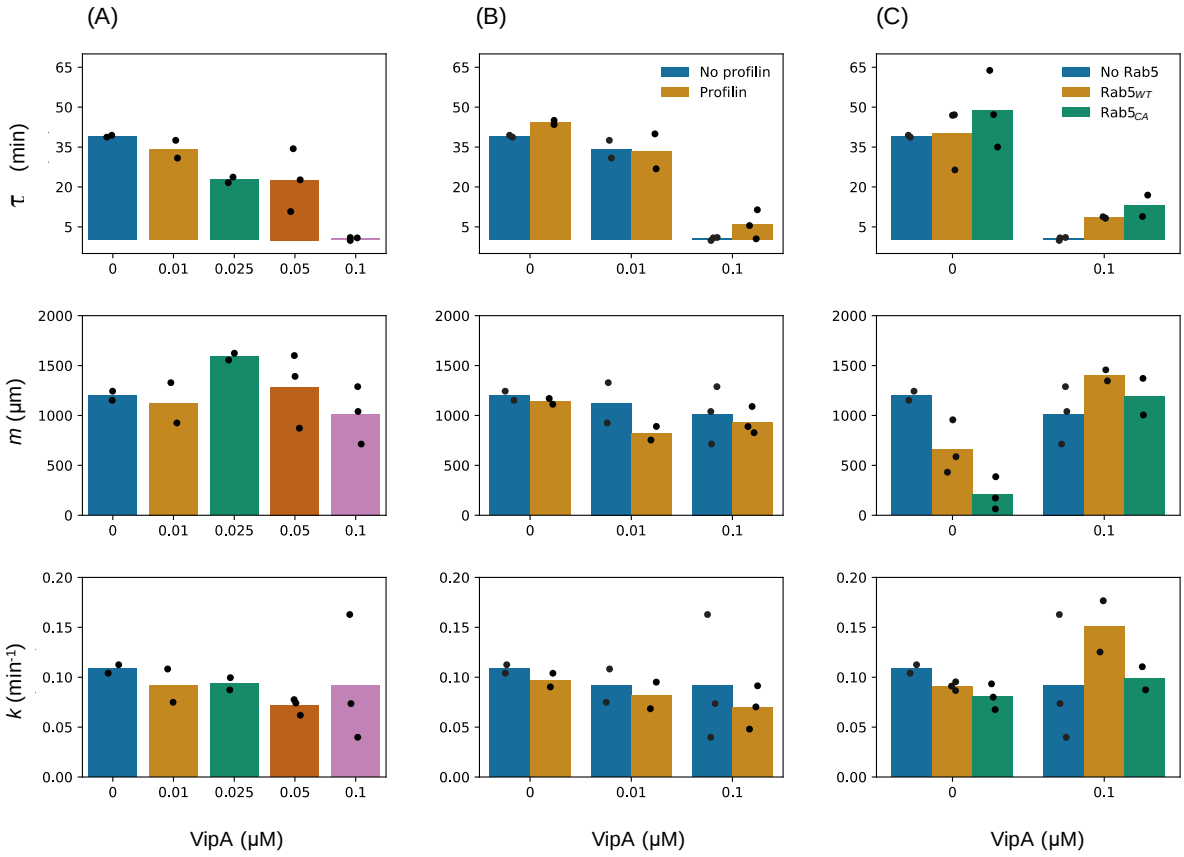

Figure 9. Calculated τ, *m* and *k* parameters after fitting of total filament length curves into a logistic function and exclusion of outlier data. τ corresponds to the time, in minutes, necessary to reach half of the maximum total filament length value and is inversely proportional to the nucleation rate; *m* corresponds to the maximum value of total filament length in μm; and *k* is proportional to the growth rate after nucleation, in min^{-1}, and is therefore proportional to the elongation rate. All three parameters define the logistic function applied for fitting the total filament length curves. Data considered as outlier were excluded (n=2–3). (A) Actin polymerization over time in the presence of different VipA concentrations. (B) Actin polymerization over time in the presence of VipA and 700 nM of profilin. (C) Actin polymerization over time in the presence of VipA and 100 nM of Rab5 (wild-type or constitutively active mutant).

A similar trend is observed in τ in the presence of both Rab5 variants, either in the absence or in the presence of VipA, as shown in Figure 9C. This indicates that Rab5 decreases the nucleation rate in both cases. A decrease of approximately 1,000 μm in the maximum of total filament length caused by the presence of $Rab5_{CA}$ is observed in the absence of VipA but

compensated by the presence of VipA. The growth rate *k* indicates that in the second case such compensation is achieved by an increasing of the elongation rate, suggesting that VipA may be implicated in actin elongation in the presence of activated Rab5 in solution. The decrease observed in *m* in the presence of both $Rab5_{WT}$ and $Rab5_{CA}$ in VipA-free conditions is due to an effect of these molecules in both actin nucleation and elongation, as evidenced by the increase in τ and the decrease in *k*. These results are consistent with a possible role for Rab5 molecules in sequestering actin monomers in solution in the absence of GTP hydrolysis. However, at a 1:1:1 actin, VipA, and Rab5 ratio, VipA is able to promote actin nucleation and, apparently, to compensate for the decrease in actin elongation caused by the active Rab5 molecules. Differences in the activity between the Rab5 variants are also suggested by these parameters although speculative, and further assays are required to validate this hypothesis.

In this attempt to kinetically characterize data resulting from time-lapse videos, it was very difficult to withdraw relevant conclusions due to high variability between replicate experiments and small sample sizes. Statistical analysis is essential for a good characterization of these parameters and valuable comparation between different conditions. However, this requires a much more representative sample size, especially considering the above-mentioned variability. Therefore, experiments must be repeated, and statistical significance of the results must be evaluated.

3.3. Generalization of the previous results by scoring of the number of filaments at 5 minutes in a more representative landscape of the sample

With the aim of characterizing the effects of VipA on actin nucleation *in vitro* in a more representative way, using the same experimental set-up as in the previously described assays, the number of filaments formed in the different conditions at approximately 5 minutes was scored following the same type of analysis. In this case, n>20 different fields of view were imaged per condition in order to obtain a more illustrative view of the sample that was not possible in the time-lapse videos, which consisted of the imaging of a single field of view over time. Since the whole imaging process takes around two minutes per condition, images were acquired in a period between 4 and 6 minutes after sample preparation. In general, this assay displayed high time-sensitivity, especially in samples with higher nucleation rates, presenting inevitable overall higher number and longer filaments by the end of the acquisition processes. Variability between fields of view was also evident during these assays. Therefore, this experiment provides important contributions towards a representative characterization of F-actin density in the sample at the beginning of the polymerization reaction, and its intrinsic drawbacks should be limited.

As proposed in the previous assay, the number of filaments formed after 5 minutes increases in the presence of VipA in a concentration-dependent fashion. Measurement of the number of filaments very soon after starting the reaction is a measurement of the nucleation rate. The nucleation rate increases monotonically with the VipA concentration, as shown in Figure 10A. These results agree with previously presented time-lapse data and confirm the role

of VipA as an actin nucleator, consistent with results from previous bulk assays (Franco et al., 2012).

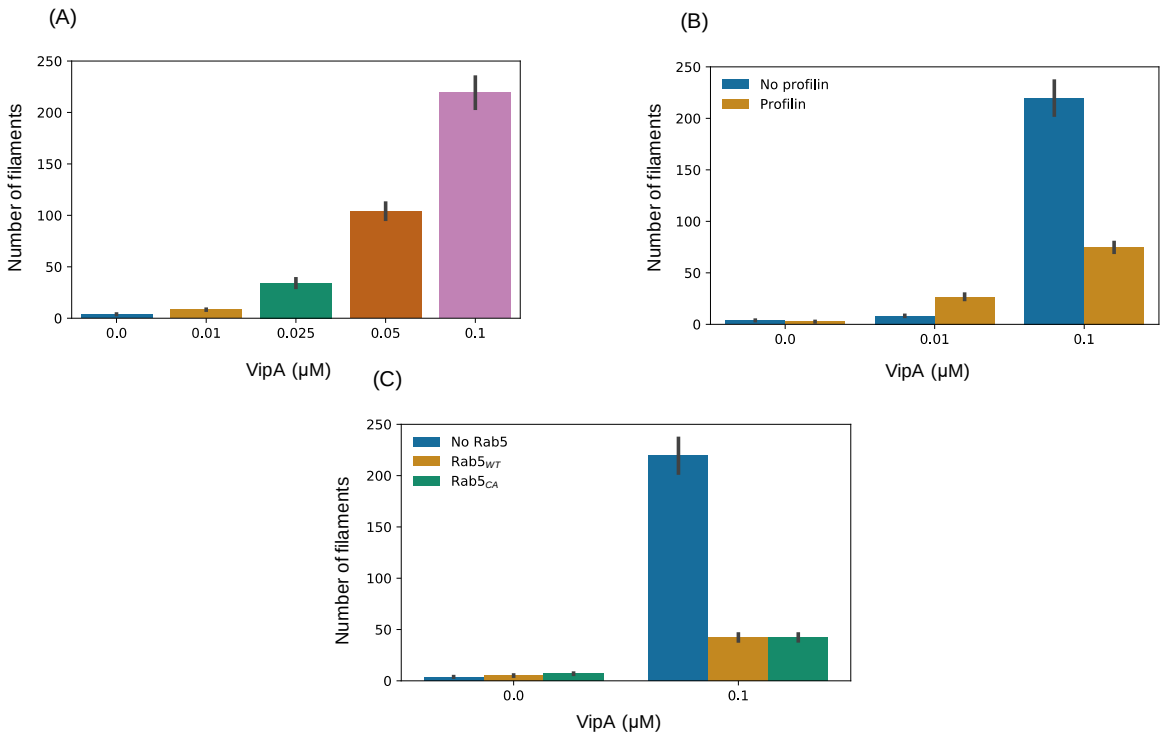

Figure 10. Number of actin filaments in different fields of view at approximately 5 minutes after sample preparation. Samples contained 100 nM of Atto 488-monomeric actin and the displayed VipA concentrations. In the corresponding cases, 100 nM of Rab5 (wild type or constitutively active mutant) or 700 nM of profilin were added to the sample. More than 20 single images of different fields of view were imaged per condition at approximately 5 min after sample preparation. Plots combine data from 3 independent replicates for each condition and correspond to the average total number of actin filaments in the presence of (A) different VipA concentrations; (B) VipA and profilin; and (C) VipA and wild type or constitutively active Rab5. The displayed gray bars correspond to a 68% confidence interval, *i. e.*, to one standard error.

In the presence of profilin, no difference is observed in the absence of VipA in terms of number of filaments formed at 5 minutes when comparing to spontaneous actin polymerization (Figure 10B). This is in agreement with previous time-lapse data, supporting that the differences observed between these conditions appear later on (Figure 7) and that the increase in τ exhibited by this condition (Figure 9B) is due to a decrease in the nucleation rate that does not display a quantitative effect at 5 minutes.

In the presence of 10 nM of VipA, however, the number of filaments is around three times higher in the presence of profilin than when VipA is absent (Figure 10B). Two out of three replicates exhibited small, but statistically significant (*p*-value = 6.9 x 10^{-9} and *p*-value = 9.5 x 10^{-11} using a two-tailed T-test) increase in nucleation in the presence of profilin. These results do not match previous time-lapse data that indicate similar actin polymerization at 5 minutes

and similar nucleation rate both in the absence and presence of profilin in this condition (Figure 7 and Figure 9B). Since it is not likely that profilin is enhancing actin nucleation or potentiating VipA-mediated nucleation at a low concentration but not at a higher concentration of the effector, it is more plausible that this difference is linked to the intrinsic time-sensitivity of the experimental set-up. The fact that one out of three replicates did not present a significant increase indicates reproducibility problems similar to those observed in the time-lapse experiments. Considering this, experiments must be repeated in order to validate these results.

The addition of profilin to the assays containing 100 nM of VipA revealed a decrease in the number of filaments scored at 5 minutes from ~ 225 to ~ 75, which corresponds to a decrease of approximately 70% in the activity of VipA on actin nucleation, as depicted in Figure 10B. These results are generally consistent with previous time-lapse data and with a role of profilin in sequestering actin monomers, thus hindering VipA's access, as previously hypothesized. These results indicate that the difference observed at 5 minutes in Figure 7 is mostly motivated by a lower number of initial filaments in the presence of profilin, and supports the previous speculation of an effect of profilin in increasing τ, indicating slower actin nucleation mediated by VipA (Figure 9B). These results demonstrate that VipA, at both 10 and 100 nM concentrations, is able to enhance actin nucleation in the presence of profilin, at least when the components are found in these proportions.

Assays performed in the presence of both wild-type and constitutively active Rab5, without VipA, indicate that nucleation at 5 minutes is similar in both absence and presence of Rab5 (Figure 10C). This is in agreement with time-lapse data presented in Figure 8 and indicates that differences observed in τ in Figure 9C appear later on. In VipA-containing conditions, a decrease in the number of filaments formed after 5 minutes from more than 200 to around 50 is observed in the presence of both wild-type and constitutively active Rab5 variants. This supports data from previous time-lapse assays and, together, these results are consistent with an effect of Rab5 in decreasing the VipA-mediated actin nucleation *in vitro*, possibly by sequestering monomeric actin. However, they do not discriminate between the two Rab5 variants, suggesting that the difference observed at 5 minutes in Figure 8 can result from an artifact created by an intrinsic variability of the system, or it can be due to higher length of the filaments formed in the presence of wild-type Rab5 at such time-point, suggesting that inhibition of VipA's activity in actin nucleation is higher in the presence of the constitutively active mutant.

3.4. Continuous uptake and pulse-chase of Dil-LDL in live HeLa cells stably expressing GFP-Rab5

To examine whether VipA has an effect on Rab5-to-Rab7 conversion in endosome maturation, colocalization between Rab5 and labeled low-density-lipoprotein (Dil-LDL) was followed over time in HeLa cells stably expressing GFP-Rab5, with and without transgenic expression of VipA.

Preliminary experiments were carried out in order to visualize Dil-LDL internalization in live cells, without performing transfection with a VipA-encoding vector. Internalization of Dil-LDL was

visible for both continuous uptake of the molecules and pulse-chase experiments. Moreover, signals for both Dil-LDL and GFP-Rab5 were fairly good through all the experiments, with minimal photobleaching (Figure 11).

At 15 minutes of Dil-LDL continuous uptake, colocalization between both components was observed, as evidenced by the arrows in Figure 11A. At 25 minutes, colocalization between these molecules started to be lost, as pointed out by the arrows. In a different cell imaged at 45 minutes, colocalization between Dil-LDL and Rab5 was similar to that observed at 25 minutes, with some remaining colocalization. In the pulse-chase experiments, images of Dil-LDL internalization do not allow tracking of the labeled lipoprotein, since medium exchanges led to transient shifts in sample positions and high fluorescence background. However, cells imaged 45 minutes after a 15-minute Dil-LDL pulse revealed little or no colocalization between Dil-LDL and GFP-Rab5 at such time-point, indicating that pulse-chase experiments are better suited for monitoring the progression of Rab5-to-Rab7 conversion (Figure 11B).

These experiments allowed testing preliminary protocols and provided relevant information for further experiments in fixed cells. The primary differences between the experiments in live cells and the following ones in fixed cells were the lack of a VipA-encoding plasmid, or empty equivalent vector, and the use of the Leibovitz's L-15 medium rather than DMEM, which was required to minimize fluorescence background and to maintain pH over longer times in the absence of a CO_2 incubator on the microscopy set-up.

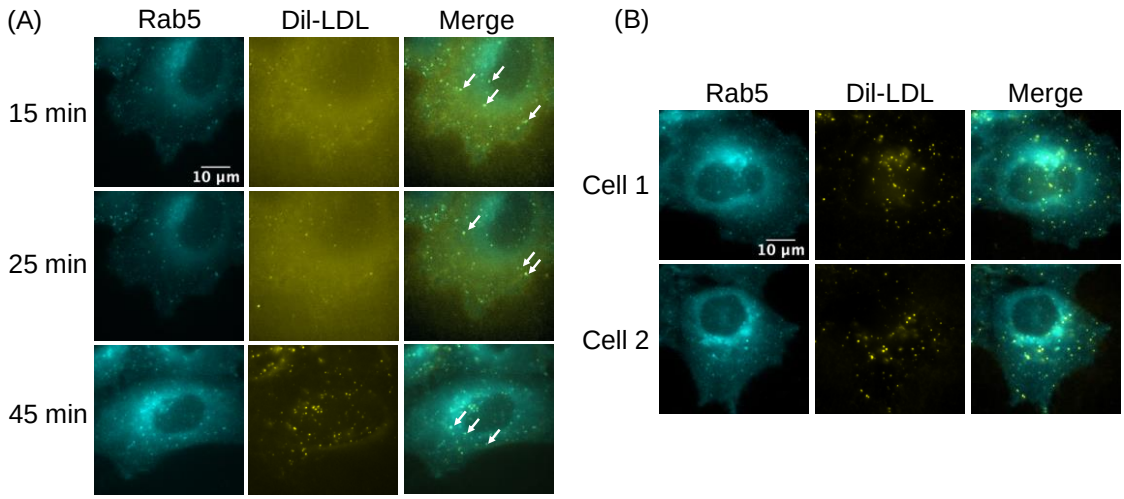

Figure 11. Dil-LDL and Rab5 colocalization in live cells. A HeLa Kyoto cell line stably expressing GFP-Rab5c was grown in complete DMEM and serum starved in 0.2% (v/v) FBS medium. Leibovitz's L-15 medium was then used to perform live-cell imaging on a widefield fluorescence microscope pre-heated to 37ºC. (A) Dil-LDL (10 µg/ml) was introduced directly in the medium and the same cell was imaged through the continuous uptake of the lipoprotein. A different cell was imaged after 45 min. (B) A 15-min pulse of 10 µg/ml Dil-LDL previously diluted and vortexed in Leibovitz's L-15 medium was applied by replacing media and after such pulse medium was replaced again by serum deficient Leibovitz's L-15 medium. Images correspond to two different cells imaged 45 min after the Dil-LDL pulse.

3.5. Colocalization between VipA and Rab5, and Dil-LDL pulse-chase in fixed HeLa cells stably expressing GFP-Rab5

To test the previous hypothesis, cells were transfected with a VipA-harboring vector or with the empty vector. After a 10-minute pulse of Dil-LDL, cells were fixed at different time-points to evaluate colocalization between GFP-Rab5 and Dil-LDL over time, to assess if such colocalization is maintained, indicating an impairment in Rab conversion.

Given the necessity of VipA visualization for selection of VipA-positive cells, the experiment was performed in fixed cells and both growth and pulse-chase protocols were informed by earlier live-cell experiments. Colocalization between the different components (Rab5, VipA, and Dil-LDL) was measured by the Manders' coefficients (see 2.6.8).

Colocalization of Alexa647-VipA with GFP-Rab5 was evident in all VipA-transfected cells (Figure 12A). Quantitative analysis revealed relatively high colocalization between the two components through all the time-points (Figure 12C). These results are consistent with previous data that showed colocalization between VipA and Rab5 in CHO cells (Franco et al., unpublished), and support the use of this cell line in future experiments. Additionally, VipA displayed a similar distribution to the one previously observed in transgenic expression of EGFP-VipA fusion in CHO cells (Bugalhão et al., 2016). An increase in VipA-Rab5 colocalization was observed 10 minutes after the Dil-LDL pulse, although no statistical significance was found for this observation (*p*-value between 0.12 and 0.17 comparing 10-minute to 0-, 20-, and 40-minute time-points using a two-tailed T-test).

The fixed cell experiment showed a huge decrease in Dil-LDL signal compared to the preliminary live-cell experiment (and Figure 12B). Although Dil-LDL was added at half the concentration in this condition, this does not account for the dramatic loss in fluorescence. Possible explanations include that the fixation, permeabilization and staining processes do not maintain the Dil-LDL signal. Particularly, permeabilization with the detergent Triton X-100 could affect lipoproteins. Keeping this difficulty in mind, colocalization analysis was performed between Rab5 signal and the weak Dil-LDL signal.

Moreover, a problem related with the number of cells emerged in this experiment and not in the experiment using live cells (3.4). The extreme difficulty in finding cells contributed to the fact that only a few were imaged per condition, requiring all data to be pooled to achieve a sufficient sample size, rather than comparing individual technical replicates. Such a problem resulted either from poor cell-adhesion to the sample chamber or to the increase in washing and medium-exchange steps undergone by the cells in this assay. All steps requiring aspiration and addition of medium should be performed with extreme caution, as this may occur. A possible solution for this could be to fix, process and label samples using a gentler fluidics system. A recently reported homebuilt system allows for rapid fixation and exchange of many solutions at a very low cost (Almada et al., 2019).

Colocalization between Dil-LDL and GFP-Rab5 exhibited lower values through all the time-points, and displayed neither a trend related to time after Dil-LDL internalization, nor difference between VipA positive and VipA-negative cells (Figure 12D). A few representative colocalization

events are evidenced by the arrows in Figure 12B. This would suggest that the lipoprotein is not notably colocalizing with Rab5 in early endosomes at any time-point, and that the presence of VipA is not interfering with the process. However, the damage observed in the Dil-LDL signal in this preliminary assay does not allow to withdraw conclusions from this quantitative analysis.

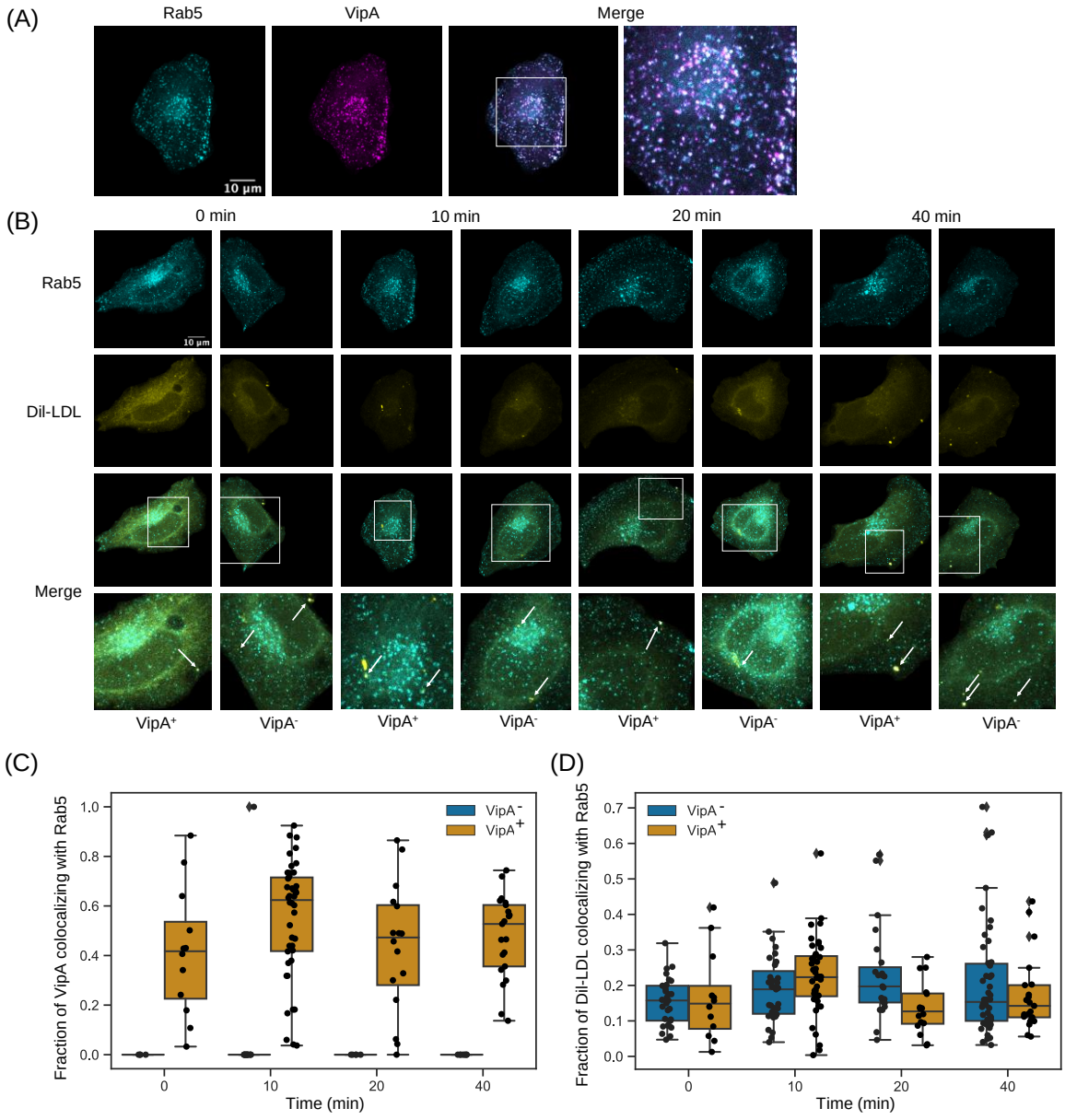

Figure 12. Colocalization of Rab5, VipA and Dil-LDL in fixed HeLa cells stably expressing GFP-Rab5c. Cells were transfected with VipA$_{WT}$-myc encoded in a mammalian transfection vector or with the empty vector, and a 10 min pulse of Dil-LDL in serum-starvation medium was applied. Cells were fixed at different time-points after the pulse. Immunostaining using conjugated antibodies was carried out for VipA visualization. (A) Representative images of colocalization between VipA and Rab5. (B) Representative images of colocalization between Dil-LDL and Rab5 at different time-points. (C) Quantitative analysis of colocalization between VipA and Rab5 measured by the Manders' coefficient for the fraction of VipA colocalizing with Rab5 in cells fixed at different time-points. (D) Quantitative analysis of colocalization

between Dil-LDL and Rab5 measured by the Manders' coefficient for the fraction of Dil-LDL colocalizing with Rab5 at different time-points. Preliminary colocalization quantitative analysis pools data from 3 technical replicates (grown and processed separately, but at the same time) due to the low number of cells (n>11).

The slightly increase in colocalization in cells harboring a VipA-encoding vector at 10 minutes can be linked to the previously observed increase in VipA-Rab5 colocalization, suggesting that LDL internalization occurs mainly at such time-point. An increase of VipA-Rab5 colocalization on early formed endosomes suggests a possible effect of VipA on endosome maturation. However, this observation remains merely speculative and the experiment must be optimized and repeated in order to evaluate these results by replication and with higher sample sizes.

4. Discussion

Using a complementary assay to directly examine actin filaments, this work reproduced previous observations that VipA promotes actin nucleation *in vitro* in a concentration-dependent manner (Franco et al., 2012). The addition of a visual component based on widefield fluorescence microscopy to the previous bulk assays introduced relevant information regarding filament number and length distribution over time as a function of the VipA concentration. Analysis of actin polymerization strongly corroborated that VipA is a *bona fide* actin nucleator *in vitro* and that the major role it plays in actin polymerization is precisely in stimulating nucleation, a rate-limiting step that is kinetically unfavorable when actin is spontaneously polymerizing (Chesarone and Goode, 2009). Results strongly suggest that VipA acts at the nucleation step rather than at elongation or disassembly of filaments, which is in accordance with previous results of *in vitro* polymerization assays (Franco et al., 2012).

The presence of profilin in the *in vitro* assays resulted in decreased actin polymerization both in the absence and the presence of VipA, consistent with profilin's role in either sequestering actin monomers and/or enhancing filament disassembly. The observed increase in τ, a parameter that is inversely proportional to the nucleation rate, as well as the decrease observed in the number of filaments formed at 5 minutes in the presence of profilin, pointed out an effect on actin nucleation, compatible with the formation of profilin-actin complexes that results in the sequestering of actin monomers and hindering of overall polymerization. An impairment in the VipA-mediated nucleation was consistent in both time-lapse experiments and scoring of the number of filaments formed at 5 minutes in different fields of view. However, VipA was still able to enhance actin nucleation in the presence of profilin in solution. These results support that VipA acts as an actin nucleator *in vivo*, as previously hypothesized (Bugalhão et al., 2016).

It remains unclear whether VipA nucleates actin monomers in the presence of profilin by recruiting profilin-actin complexes or through a competition mechanism to bind the actin monomer. One hypothesis is that VipA and profilin compete for the binding-site in the actin monomer, implying that VipA binds to actin at its barbed face. Yet, even if the binding site is not shared, the presence of profilin may interfere with the correct positioning of VipA along the actin monomer, thus leaving it in a non-fully active or inactive state. The requirement of direct interaction between VipA and profilin through the proline-rich motif of VipA does not seem probable since VipA mutants lacking this motif were able to induce a defective vacuolar trafficking in yeast, a process that is most likely linked to its ability to hijack the actin network (Bugalhão et al., 2016). Notwithstanding, it is not possible to discard the possibility that some actin monomers did not form complexes with profilin, and that these observations merely reflect the regular binding of VipA to the remaining free actin monomers.

Previous co-immunoprecipitation and colocalization assays in Chinese hamster epithelial cells demonstrated that VipA interacts and colocalizes with the small Rab5 GTPase, an early endosome marker (Franco et al., unpublished). This motivated experiments to assess the

impact of active Rab5 GTPase on the *in vitro* actin nucleation. A decrease in actin polymerization was observed, both in the nucleation and the elongation steps. This suggests a role for Rab5 GTPase in binding to actin monomers, sequestering them in conditions with none or poor GTP hydrolysis. An impairment in the VipA-mediated actin nucleation is shown by an increase of τ in the time-lapse data, which indicates a slower nucleation rate, and a strong decrease in the number of filaments formed at 5 minutes in different fields of view. However, VipA was able to enhance nucleation in the presence of Rab5 in solution. Moreover, in the presence of the bacterial effector, the effects of Rab5 on the polymerization rate, *k*, and on the maximum total filament length, *m*, decreased, suggesting that VipA may play a role in actin elongation in the presence of Rab5.

It is not clear how VipA binds Rab5, although it has been previously hypothesized that it does so through the N-terminal region, since mutants lacking this portion do not colocalize with early endosomes *in vivo* (Bugalhão et al., 2016), and mutants lacking the C-terminal region were still able to bind Rab5 *in vitro* (Franco et al., unpublished). These results raised the hypothesis that VipA interacts with both Rab5 on early endosomes and its associated actin cytoskeleton *in vivo*, leading to a disruption of endosome trafficking by hijacking the actin network. A role for GTP-binding and GTP-hydrolysis in Rab5's effects on actin polymerization and VipA-mediated nucleation *in vitro* remains unclear. Moreover, the consistent higher effect of the constitutively active mutant in impairing actin polymerization suggests that GTPγS-binding to Rab5 molecules was not completely efficient.

The previously demonstrated colocalization between Rab5 GTPase and VipA in Chinese hamster epithelial cells, together with additional evidence presented in this *in vitro* work concerning a possible role for VipA in destabilizing Rab5 functions, raised the possibility of VipA acting as a disruptor of Rab5 to Rab7 conversion, and therefore as a blocker of endosome maturation. An experimental framework based on previous work from Rink et al., 2005, was established, consisting of the tracking of colocalization between stably expressed fluorescent Rab5 and an internalized fluorescently labeled lipoprotein to assess whether there was a preservation of such colocalization over time in VipA-transfected cells, which would indicate an impairment of Rab conversion. Despite technical problems that lead to significant damage of the Dil-LDL signal, preliminary results support that it is a good model for further studies on this topic with some optimization.

High levels of colocalization between Alexa647-VipA and GFP-Rab5 expressed by the cells were obtained, suggesting that this cell line has the potential to be useful for additional studies of the effects of VipA on the activity of Rab5 *in vivo*, with the great advantage of stably expressing fluorescent Rab5. It should however be noted that it may not be a good and reproducible model for infection studies, since *Legionella* hosts are typically phagocytic cells that may display properties that these HeLa cells do not. An increase of both VipA-Rab5 and Dil-LDL-Rab5 colocalization was noticed at 10 minutes after the Dil-LDL pulse, although with no statistical significance. However, this increase suggests a maximum of Dil-LDL internalization at

10 minutes and a maximum colocalization between VipA and Rab5 at this time-point, consistent with a role for VipA in endosome maturation.

Altogether, these results corroborate previous data indicating that VipA is a strong actin nucleator *in vitro* and that it acts as an actin nucleator in the presence of profilin as well. This suggests that it acts as an actin nucleator *in vivo*, since it is believed that profilin-actin is the most abundant form of monomeric actin in cells. It is still unclear where and when VipA acts inside the host cell during infection, but evidence of both its impact in destabilizing the effect of Rab5 on actin polymerization *in vitro*, and the strong colocalization between VipA and Rab5 in HeLa cells, provided new insight regarding this subject, raising the hypothesis that VipA may be acting on the F-actin network associated with early endosomes by interacting with both Rab5 and actin. The physiological relevance that this may have in the *Legionella* host cells remains speculative. However, the linkage between the actin cytoskeleton and the endocytic pathway suggests a mechanism through which VipA hijacks the host actin network to disrupt endocytosis. It remains unknown whether VipA is implicated in endosome maturation disruption and if it is able to yield a phenotype that can be relatable with the formation of the specialized phagosome LCV.

Given that the effects of VipA on actin nucleation are clear in the absence of additional proteins, and that it apparently recruits actin monomers *in vitro* even in the presence of other actin-binding proteins that may be significantly decreasing the availability of free monomeric actin, VipA seems to display the same *modus operandi* of known nucleators, such as Spire, Cobl, or Lmod. These nucleators recruit and align actin monomers without the requirement of additional proteins, generating a stable polymerization “seed” (Ahuja et al., 2007; Bosch et al., 2007; Chereau et al., 2008). The predicted coiled-coil region (Bugalhão et al., 2016), a motif known to participate in protein-protein interactions, may play a role in the interaction between different actin-carrying VipA molecules, positioning actin monomers together and stabilizing the intrinsically unstable dimeric and trimeric intermediates.

5. Conclusions and future work

In this work we reproduced and reinforced previous studies that identified the *Legionella* VipA bacterial effector as an actin nucleator, by incorporating microscopy data that allows a better understanding of F-actin distribution over time both in number and length. VipA strongly enhanced *in vitro* actin polymerization and such enhancement occurred mainly in the nucleation step. Moreover, we provide evidence that VipA nucleates actin *in vitro* in the presence of profilin, which can be extrapolated to a strong nucleation capacity *in vivo* since this protein is abundantly found in complex with monomeric actin in cells. We also characterized the effects of the presence of active Rab5 GTPase on the *in vitro* actin polymerization, which suggested that these molecules bind to actin monomers and sequester them at least in the absence of GTP hydrolysis. Additionally, VipA enhanced actin nucleation in the presence of active Rab5, raising the hypothesis of a mechanistic operational role for VipA *in vivo* in which it colocalizes and binds to Rab5 on early endosomes, and also binds to monomeric actin, promoting a destabilization of the Rab5-associated actin network. Consistent with this, we found that VipA colocalizes with GFP-Rab5 stably expressed in HeLa cells.

Despite new insights in this work, efforts must be made to improve the quality and reproducibility of the assays in order to validate the obtained results and acquire more information. For instance, *in vitro* assays should be performed in order to visualize polymerization from the beginning of the reaction, since in the presence of VipA it occurs very rapidly, and information is lost by missing the first five minutes. This would require an automated system, which could perhaps be achieved by the assembly of a fluidics system to the microscope that would mix components to start the reaction and introduce it in a chamber for visualization in a much faster way than it is possible with human manipulation. Scoring of filaments in different fields of view at a specific time-point would also benefit from automation, since the performed assays displayed high time-sensitivity.

Besides rapidity, it is likely that an automated system would reduce variability between samples, which constituted the largest challenge in this work. Improving image quality is also important, especially in terms of filaments binding to the surface. However, this comes with a tradeoff, since it depends on tethering proteins and interaction between these and the sample components must be avoided in order to prevent interference with the results. Therefore, other proteins to perform this function should be tested, and different concentration ranges of such proteins should be studied to completely rule out possible impact on the results.

Improvements in image quality and sample manipulation would allow the tracking of individual filaments and thus the establishment of a more accurate kinetic growth model which could clarify whether VipA plays a role in actin elongation. Increasing the acquisition rate of the time-lapse videos could also ease filament tracking. Additionally, a better system for filament detection that could accurately and unambiguously distinguish between overlapping filaments even at high densities would be a relevant improvement in this direction. Given the high

variability observed, experiment repeats are necessary and further statistical analysis is required to determine reliability and significance of the results.

Regardless of the above-mentioned limitations of the current experimental set-up, these results raised several hypotheses that are worth validating in the future through the same and/or different approaches.

It would be interesting to work with a range of presumable actin-profilin complexes similar to physiological concentrations, 10-80 μM (Pernier et al., 2016), in order to determine the necessary VipA concentrations to maintain a strong nucleator activity in cells.

In vitro assays similar to those presented in this work may contribute to the identification of a Rab5 GTPase binding-site in the VipA structure and to a possible mechanism of interaction between VipA and Rab5 on early endosomes. Activation of Rab5 by nucleotide exchange to GTPγS should be optimized in order to obtain similar effects between the wild-type and constitutively active variants. A different approach is to prepare the active forms of Rab5 before the elution steps of the purification procedure, with GST-Rab5 coated glutathione-sepharose beads immobilized in the chromatography column, as described by Murray and Backer, 2005. Additionally, the utilization of Rab5 forms prior to loading with the non-hydrolysable GTP analog would be important for a better understanding of the importance of GTP binding and hydrolysis in the activity of this GTPase on actin and its interaction with VipA *in vitro*.

To better understand if VipA interacts with both Rab5 and its associated actin network in cells, it would be important to characterize *in vitro* its ability to promote actin nucleation in the presence of eukaryotic proteins known to be involved in the process in physiological conditions, especially in the presence of annexin A2 and spire, which were found to be responsible for the nucleation of the Rab5-associated actin filaments (Muriel et al., 2017). Moreover, the experiments carried out in HeLa cells should be repeated, and additions such as visualization of F-actin should be attempted.

The technical difficulties encountered in the preliminary experiments in HeLa cells can be addressed by modifying cell growth and fixation protocols. With further optimization, this is a worthwhile experimental framework to test how VipA affects endosome maturation. It can also be extended to address VipA-Rab5 interactions with advanced microscopy methods such as super-resolution microscopy or fluorescence resonance energy transfer (FRET) to examine how VipA and Rab5 interact *in vivo*.

Besides, a new strategy to overcome the problem of the inability to differentiate between non-transfected cells and cells transfected with the original vector is required. Both the empty and VipA-expressing vectors could be modified to express a cyan fluorescent protein, and GFP-Rab5 could be replaced by YFP-Rab5. This would allow for 3-color imaging (yellow Rab5, orange Dil-LDL, and red VipA) after first selecting for cells harboring a similar number of plasmids based on their level of cyan fluorescence. This modification would also allow upgraded live-cell imaging, although medium exchange would still be required and therefore an improved system would be necessary.

The experiments carried out in this work opened a new path in the investigation of the physiological relevance of the VipA bacterial effector by introducing new approaches to this subject that, with the required improvements, will certainly provide valuable insight towards the understanding of the mechanisms of VipA in altering actin dynamics during infection by *L. pneumophila*.

6. References

Ahuja, R., Pinyol, R., Reichenbach, N., Custer, L., Klingensmith, J., Kessels, M.M., and Qualmann, B. (2007). Cordon-bleu is an actin nucleation factor and controls neuronal morphology. Cell *131*, 337–350.

Almada, P., Pereira, P.M., Culley, S., Caillol, G., Boroni-Rueda, F., Dix, C.L., Charras, G., Baum, B., Laine, R.F., Leterrier, C., et al. (2019). Automating multimodal microscopy with NanoJ-Fluidics. Nat. Commun. *10*, 1–9.

Armstrong, B.Y.J.A., and Hart, A.P.D.A. (1971). Response of cultured macrophages to *mycobacterium tuberculosis*, with observations on fusion of lysosomes with phagosomes. J. Exp. Med. *134*, 713–740.

Babst, M., Odorizzi, G., Estepa, E.J., and Emr, S.D. (2000). Mammalian tumor susceptibility gene 101 (TSG101) and the yeast homologue, Vps23p, both function in late endosomal trafficking. Traffic. *1*, 248–258.

Barbero, P., Bittova, L., and Pfeffer, S.R. (2002). Visualization of Rab9-mediated vesicle transport from endosomes to the trans-Golgi in living cells. J. Cell Biol. *156*, 511–518.

Barbieri, M.A., Li, G., Colombo, M.I., and Stahl, P.D. (1994). Rab5, an early acting endosomal GTPase, supports in vitro endosome fusion without GTP hydrolysis. J. Biol. Chem. *269*, 18720–18722.

Barrabeig, I., Rovira, A., Garcia, M., Oliva, J.M., Vilamala, A., Ferrer, M.D., Sabriá, M., and Domínguez, A. (2010). Outbreak of Legionnaires' disease associated with a supermarket mist machine. Epidemiol. Infect. *138*, 1823–1828.

Bencini, M.A., Yzerman, E.P.F., Koornstra, R.H.T., Nolte, C.C.M., Den Boer, J.W., and Bruin, J.P. (2005). A case of Legionnaires' disease caused by aspiration of ice water. Arch. Environ. Occup. Heal. *60*, 302–306.

Bennett, E., Ashton, M., Calvert, N., Chaloner, J., Cheesbrough, J., Egan, J., Farrell, I., Hall, I., Harrison, T.G., Naik, F.C., et al. (2014). Barrow-in-Furness: A large community legionellosis outbreak in the UK. Epidemiol. Infect. *142*, 1763–1777.

Den Boer, J.W., Yzerman, E.P.F., Schellekens, J., Lettinga, K.D., Boshuizen, H.C., Van Steenbergen, J.E., Bosman, A., Van Hof, S. Den, Van Vliet, H.A., Peeters, M.F., et al. (2002). A large outbreak of Legionnaires' disease at a flower show, the Netherlands, 1999. Emerg. Infect. Dis. *8*, 37–43.

Bolte, S., and Cordelières, F.P. (2006). A guided tour into subcellular colocalization analysis in light microscopy. J. Microsc. *224*, 213–232.

Borges, V., Nunes, A., Sampaio, D.A., Vieira, L., Machado, J., Simões, M.J., Gonçalves, P., and Gomes, J.P. (2016). *Legionella pneumophila* strain associated with the first evidence of person-to-person transmission of Legionnaires' disease: a unique mosaic genetic backbone. Sci. Rep. *6*, 1–11.

Bosch, M., Le, K.H.D., Bugyi, B., Correia, J.J., Renault, L., and Carlier, M.F. (2007). Analysis of the function of spire in actin assembly and its synergy with formin and profilin. Mol. Cell *28*,

555–568.

Bowers, K., and Stevens, T.H. (2005). Protein transport from the late Golgi to the vacuole in the yeast Saccharomyces cerevisiae. Biochim. Biophys. Acta *1744*, 438–454.

Brady, M.J., Campellone, K.G., Ghildiyal, M., and Leong, J.M. (2007). Enterohaemorrhagic and enteropathogenic *Escherichia coli* Tir proteins trigger a common Nck-independent actin assembly pathway. Cell. Microbiol. *9*, 2242–2253.

Bugalhão, J.N., Mota, L.J., and Franco, I.S. (2016). Identification of regions within the *Legionella pneumophila* VipA effector protein involved in actin binding and polymerization and in interference with eukaryotic organelle trafficking. Microbiologyopen *5*, 118–133.

Bugyi, B., and Carlier, M.F. (2010). Control of actin filament treadmilling in cell motility. Annu. Rev. Biophys. *39*, 449–470.

Carlsson, L., Nyström, L.E., Sundkvist, I., Markey, F., and Lindberg, U. (1977). Actin polymerizability is influenced by profilin, a low molecular weight protein in non-muscle cells. J. Mol. Biol. *115*, 465–483.

Charpentier, X., Gabay, J.E., Reyes, M., Zhu, J.W., Weiss, A., and Shuman, H.A. (2009). Chemical genetics reveals bacterial and host cell functions critical for type IV effector translocation by *Legionella pneumophila*. PLoS Pathog. *5*, e1000501.

Chen, J., Felipe, K.S. De, Clarke, M., Lu, H., Roger, O., Segal, G., and Shuman, H.A. (2004). *Legionella* effectors that promote nonlytic release from protozoa. Science *303*, 1358–1361.

Chen, J., Reyes, M., Clarke, M., and Shuman, H.A. (2007). Host cell-dependent secretion and translocation of the LepA and LepB effectors of *Legionella pneumophila*. Cell. Microbiol. *9*, 1660–1671.

Chereau, D., Boczkowska, M., Skwarek-Maruszewska, A., Fujiwara, I., Hayes, D.B., Rebowski, G., Lappalainen, P., Pollard, T.D., and Dominguez, R. (2008). Leiomodin is an actin filament nucleator in muscle cells. Science *320*, 239–243.

Chesarone, M.A., and Goode, B.L. (2009). Actin nucleation and elongation factors: mechanisms and interplay. Curr. Opin. Cell Biol. *21*, 28–37.

Chidiac, C., Che, D., Pires-Cronenberger, S., Jarraud, S., Campèse, C., Bissery, A., Weinbreck, P., Brun-Buisson, C., Sollet, J.P., Ecochard, R., et al. (2012). Factors associated with hospital mortality in community-acquired legionellosis in France. Eur. Respir. J. *39*, 963–970.

Le Clainche, C., and Carlier, M.F. (2008). Regulation of actin assembly associated with protrusion and adhesion in cell migration. Physiol. Rev. *88*, 489–513.

Colville, A., Crowley, J., Dearden, D., Slack, R.C.B., and Lee, J.V. (1993). Outbreak of Legionnaires' disease at University Hospital, Nottingham. Epidemiology, microbiology and control. Epidemiol. Infect. *110*, 105–116.

Cowles, C.R., Snyder, W.B., Burd, C.G., and Emr, S.D. (1997). Novel Golgi to vacuole delivery pathway in yeast: identification of a sorting determinant and required transport component. EMBO J. *16*, 2769–2782.

Cunha, B.A. (2008). Atypical pneumonias: current clinical concepts focusing on Legionnaires' disease. Curr. Opin. Pulm. Med. *14*, 183–194.

Darsow, T., Odorizzi, G., and Emr, S.D. (2000). Invertase fusion proteins for analysis of protein trafficking in yeast. Methods Enzymol. *327*, 95–106.

Debroy, S., Dao, J., Söderberg, M., Rossier, O., and Cianciotto, N.P. (2006). *Legionella pneumophil*a type II secretome reveals unique exoproteins and a chitinase that promotes bacterial persistence in the lung. Proc. Natl. Acad. Sci. U. S. A. *103*, 19146–19151.

European Bioinformatics Institute (EMBL-EBI) (1996). UniProtKB P20339_RAB5A_HUMAN. UniProt. Retrieved from https://www.uniprot.org/uniprot/P20339 on October 4, 2019.

European Bioinformatics Institute (EMBL-EBI) (2004). UniProtKB Q5ZYI2_LEGPH. UniProt. Retrieved from https://www.uniprot.org/uniprot/Q5ZYI2 on October 4, 2019.

European Center for Disease Prevention and Control (ECDC) (2013). Legionnaires' disease in Europe, 2011.

European Center for Disease Prevention and Control (ECDC) (2019). Legionnaires' disease. ECDC Annual epidemiological report for 2017.

Egile, C., Loisel, T.P., Laurent, V., Li, R., Pantaloni, D., Sansonetti, P.J., and Carlier, M. (1999). Activation of the CDC42 effector N-WASP by the *Shigella flexneri* IcsA protein promotes actin nucleation by Arp2/3 complex and bacterial actin-based motility. J. Cell Biol. *146*, 1319–1332.

Feyder, S., De Craene, J.O., Bär, S., Bertazzi, D.L., and Friant, S. (2015). Membrane trafficking in the yeast *Saccharomyces cerevisiae* model. Int. J. Mol. Sci. *16*, 1509–1525.

Fields, B.S., Benson, R.F., and Besser, R.E. (2002). *Legionella* and Legionnaires' disease: 25 years of investigation. Clin. Microbiol. Rev. *15*, 506–526.

Franco, I.S., Shuman, H.A., and Charpentier, X. (2009). The perplexing functions and surprising origins of *Legionella pneumophila* type IV secretion effectors. Cell. Microbiol. *11*, 1435–1443.

Franco, I.S., Shohdy, N., and Shuman, H.A. (2012). The *Legionella pneumophila* effector VipA is an actin nucleator that alters host cell organelle trafficking. PLoS Pathog. *8*, e1002546.

Franke, C., Repnik, U., Segeletz, S., Brouilly, N., Kalaidzidis, Y., Verbavatz, J., and Zerial, M. (2019). Correlative single-molecule localization microscopy and electron tomography reveals endosome nanoscale domains. Traffic. *20*, 601–617.

Friis, R.R. (1972). Interaction of L cells and *Chlamydia psittaci*: entry of the parasite and host responses to its development. J. Bacteriol. *110*, 706–721.

Gao, L.Y., Harb, O.S., and Kwaik, Y.A. (1997). Utilization of similar mechanisms by L*egionella pneumophila* to parasitize two evolutionarily distant host cells, mammalian macrophages and protozoa. Infect. Immun. *65*, 4738–4746.

Garau, J., Fritsch, A., Arvis, P., and Read, R.C. (2010). Clinical efficacy of moxifloxacin versus comparator therapies for community-acquired pneumonia caused by *Legionella* spp. J. Chemother. *22*, 264–266.

García-fulgueiras, A., Navarro, C., Fenoll, D., García, J., González-diego, P., Jiménez-buñuales, T., Rodriguez, M., Lopez, R., Pacheco, F., Ruiz, J., et al. (2003). Legionnaires' disease outbreak in Murcia, Spain. Emerg. Infect. Disease *9*, 915–921.

Garrido, R.M.B., Parra, F.J.E., Frances, L.A., Guevara, R.M.R., Sanchez-Nieto, J.M.,

Hernandez, M.S., Martinez, J.A.S., and Huerta, F.H. (2005). Antimicrobial chemotherapy for Legionnaires' disease: Levofloxacin versus Macrolides. Clin. Infect. Dis. *40*, 800–806.

Gertler, F.B., Niebuhr, K., Reinhard, M., Wehland, J., and Soriano, P. (1996). Mena, a relative of VASP and *Drosophila* enabled, is implicated in the control of microfilament dynamics. Cell *87*, 227–239.

Goldschmidt-Clermont, P.J., Furman, M.I., Wachsstock, D., Safer, D., Nachmias, V.T., and Pollard, T.D. (1992). The control of actin nucleotide exchange by thymosinβ4 and profilin. A potential regulatory mechanism for actin polymerization in cells. Mol. Biol. Cell *3*, 1015–1024.

Gomez-Valero, L., and Buchrieser, C. (2019). Intracellular parasitism, the driving force of evolution of *Legionella pneumophila* and the genus *Legionella*. Genes Immun. *20*, 394–402.

Graells, T., Ishak, H., Larsson, M., and Guy, L. (2018). The all-intracellular order *Legionellales* is unexpectedly diverse, globally distributed and lowly abundant. FEMS Microbiol. Ecol. *94*, 1–14.

Greig, J.E., Carnie, J.A., Tallis, G.F., Ryan, N.J., Tan, A.G., Gordon, I., Zwolak, B., Leydon, J.A., Guest, C.S., and Hart, W.G. (2004). An outbreak of Legionnaires' disease at the Melbourne Aquarium, April 2000: Investigation and case-control studies. Med. J. Aust. *180*, 566–572.

Griffin, A.T., Peyrani, P., Wiemken, T., and Arnold, F. (2010). Macrolides versus quinolones in *Legionella pneumonia*: results from the Community-Acquired Pneumonia Organization international study. Int. J. Tuberc. Lung Dis. *14*, 495–499.

Griffiths, G., and Gruenberg, J. (1991). The arguments for pre-existing early and late endosomes. Trends Cell Biol. *1*, 5–9.

Gruenheid, S., DeVinney, R., Bladt, F., Goosney, D., Gelkop, S., Gish, G.D., Pawson, T., and Finlay, B.B. (2001). Enteropathogenic *E. coli* Tir binds Nck to initiate actin pedestal formation in host cells. Nat. Cell Biol. *3*, 856–859.

Guo, Z., Stephenson, R., Qiu, J., Zheng, S., and Luo, Z.Q. (2014). A *Legionella* effector modulates host cytoskeletal structure by inhibiting actin polymerization. Microbes Infect. *16*, 225–236.

Haranaga, S., Tateyama, M., Higa, F., Miyagi, K., Akamine, M., Azuma, M., Yara, S., Koide, M., and Fujita, J. (2007). Intravenous ciprofloxacin versus erythromycin in the treatment of *Legionella pneumonia*. Intern. Med. *46*, 353–357.

Harrison, T.G., Dournon, E., and Taylor, A.G. (1987). Evaluation of sensitivity of two serological tests for diagnosing pneumonia caused by Legionella pneumophila serogroup 1. J. Clin. Pathol. *40*, 77–82.

He, H.J., Wang, X.S., Pan, R., Wang, D.L., Liu, M.N., and He, R.Q. (2009). The proline-rich domain of tau plays a role in interactions with actin. BMC Cell Biol. *10*:81.

He, L., Lin, Y., Ge, Z. huang, He, S. yu, Zhao, B. bei, Shen, D., He, J. guo, and Lu, Y. jun (2019). The *Legionella pneumophila* effector WipA disrupts host F-actin polymerization by hijacking phosphotyrosine signalling. Cell Microbiol. *21*, e13014.

Helbig, H., Uldum, S.A., Bernander, S., Lu, P.C., Abraham, B., Gaia, V., and Harrison, T.G.

(2003). Clinical utility of urinary antigen detection for diagnosis of Legionnaires' disease. Society *41*, 838–840.

Horwitz, M.A. (1983a). Formation of a novel phagosome by the legionnaires' disease bacterium (*Legionella pneumophila*) in human monocytes. J. Exp. Med. *158*, 1319–1331.

Horwitz, M.A. (1983b). The legionnaires' disease bacterium (*Legionella pneumophila*) inhibits phagosome-lysosome fusion in human monocytes. J. Exp. Med. *158*, 2108–2126.

Horwitz, M.A. (1984). Phagocytosis of the legionnaires' disease bacterium (*Legionella pneumophila*) occurs by a novel mechanism: engulfment within a pseudopod coil. Cell *36*, 27–33.

Horwitz, M.A., and Maxfield, F.R. (1984). *Legionella pneumophila* inhibits acidification of its phagosome in human monocytes. J. Cell Biol. *99*, 1936–1943.

Huotari, J., and Helenius, A. (2011). Endosome maturation. EMBO J. *30*, 3481–3500.

Isberg, R.R., O'Connor, T.J., and Heidtman, M. (2009). The *Legionella pneumophila* replication vacuole: making a cosy niche inside host cells. Nat. Rev. Microbiol. *7*, 13–24.

Jones, T.C., and Hirsch, J.G. (1972). The interaction between *Toxoplasma gondii* and mammalian cells. II. The absence of lysosomal fusion with phagocytic vacuoles containing living parasites. J. Exp. Med. *136*, 1173–1194.

Kagan, J.C., and Roy, C.R. (2002). *Legionella* phagosomes intercept vesicular traffic from endoplasmic reticulum exit sites. Nat. Cell Biol. *4*, 945–954.

Kimple, M.E., Brill, A.L., and Pasker, R.L. (2013). Overview of affinity tags for protein purification. Curr. Protoc. Protein Sci. *73*:Unit 9.9.

Kocks, C., Gouin, E., Tabouret, M., Berche, P., Ohayon, H., and Cossart, P. (1992). *L. monocytogenes*-induced actin assembly requires the *actA* gene product, a surface protein. Cell *68*, 521–531.

Krishnan, K., and Moens, P.D.J. (2009). Structure and functions of profilins. Biophys. Rev. *1*, 71–81.

Lesser, C.F., and Miller, S.I. (2001). Expression of microbial virulence proteins in *Saccharomyces cerevisiae* models mammalian infection. EMBO J. *20*, 1840–1849.

Levy, M.L., Jeune, I. Le, Woodhead, M.A., Macfarlane, J.T., and Lim, W.S. (2010). Primary care summary of the British Thoracic Society guidelines for the management of community acquired pneumonia in adults: 2009 Update. Prim. Care Respir. J. *19*, 21–27.

Lifshitz, Z., Burstein, D., Peeri, M., Zusman, T., Schwartz, K., Shuman, H.A., Pupko, T., and Segal, G. (2013). Computational modeling and experimental validation of the *Legionella* and *Coxiella* virulence-related type-IVB secretion signal. Proc. Natl. Acad. Sci. U. S. A. *110*, E707-715.

Lindsay, D.S.J., Brown, A.W., Brown, D.J., Pravinkumar, S.J., Anderson, E., and Edwards, G.F.S. (2012). *Legionella longbeachae* serogroup 1 infections linked to potting compost. J. Med. Microbiol. *61*, 218–222.

Liu, Y., Zhu, W., Tan, Y., Nakayasu, E.S., Staiger, C.J., and Luo, Z.Q. (2019). A *Legionella* Effector Disrupts Host Cytoskeletal Structure by Cleaving Actin. Cell Microbiol. *21*, 1–23.

Lugagne, J.-B., Lin, H., and Dunlop, M.J. (2019). DeLTA: automated cell segmentation, tracking, and lineage reconstruction using deep learning. BioRxiv (720615) [Preprint]. Available from https://doi.org/10.1101/720615.

Luo, Z.Q., and Isberg, R.R. (2004). Multiple substrates of the *Legionella pneumophila* Dot/Icm system identified by interbacterial protein transfer. Proc. Natl. Acad. Sci. U. S. A. *101*, 841–846.

Mandell, L.A., Wunderink, R.G., Anzueto, A., Bartlett, J.G., Campbell, G.D., Dean, N.C., Dowell, S.F., File, T.M., Musher, D.M., Niederman, M.S., et al. (2007). Infectious Diseases Society of America/American Thoracic Society consensus guidelines on the management of community-acquired pneumonia in adults. Clin. Infect. Dis. *44*, S27–S72.

Marra, A., Blander, S.J., Horwitz, M.A., and Shuman, H.A. (1992). Identification of a *Legionella pneumophila* locus required for intracellular multiplication in human macrophages. Proc. Natl. Acad. Sci. U. S. A. *89*, 9607–9611.

Mentasti, M., Fry, N.K., Afshar, B., Palepou-Foxley, C., Naik, F.C., and Harrison, T.G. (2012). Application of *Legionella pneumophila*-specific quantitative real-time PCR combined with direct amplification and sequence-based typing in the diagnosis and epidemiological investigation of Legionnaires' disease. Eur. J. Clin. Microbiol. Infect. Dis. *31*, 2017–2028.

Michard, C., Sperandio, D., Baïlo, N., Pizarro-Cerdá, J., LeClaire, L., Chadeau-Argaud, E., Pombo-Grégoire, I., Hervet, E., Vianney, A., Gilbert, C., et al. (2015). The *Legionella* kinase legk2 targets the arp2/3 complex to inhibit actin nucleation on phagosomes and allow bacterial evasion of the late endocytic pathway. MBio *6*, 1–14.

Mier, P., Alanis-Lobato, G., and Andrade-Navarro, M.A. (2017). Protein-protein interactions can be predicted using coiled coil co-evolution patterns. J. Theor. Biol. *412*, 198–203.

Muriel, O., Tomas, A., Scott, C.C., and Gruenberg, J. (2016). Moesin and cortactin control actin-dependent multivesicular endosome biogenesis. Mol. Biol. Cell *27*, 3305–3316.

Muriel, O., Scott, C.C., Larios, J., Mercier, V., and Gruenberg, J. (2017). In vitro polymerization of F-actin on early endosomes. J. Vis. Exp. 1–9.

Murphy, R.F. (1991). Maturation models for endosome and lysosome biogenesis. Trends Cell Biol. *1*, 77–82.

Murray, J.T., and Backer, J.M. (2005). Analysis of hVps34/hVps15 interactions with Rab5 in vivo and in vitro. Methods Enzymol. *403*, 789–799.

Mykietiuk, A., Carratala, J., Fernandez-Sabe, N., Dorca, J., Verdaguer, R., Manresa, F., and Gudiol, F. (2005). Clinical outcomes for hospitalized patients with *Legionella* pneumonia in the antigenuria era: the influence of Levofloxacin therapy. Clin. Infect. Dis. *40*, 794–799.

Narita, A. (2011). Minimum requirements for the actin-like treadmilling motor system. Bioarchitecture *1*, 205–208.

O'Connor, T.J., Adepoju, Y., Boyd, D., and Isberg, R.R. (2011). Minimization of the *Legionella pneumophila* genome reveals chromosomal regions involved in host range expansion. Proc. Natl. Acad. Sci. U. S. A. *108*, 14733–14740.

O'Loughlin, R.E., Kightlinger, L., Werpy, M.C., Brown, E., Stevens, V., Hepper, C., Keane, T.,

Benson, R.F., Fields, B.S., and Moore, M.R. (2007). Restaurant outbreak of Legionnaires' disease associated with a decorative fountain: an environmental and case-control study. BMC Infect. Dis. *7*, 1–9.

Odorizzi, G., Cowles, C.R., and Emr, S.D. (1998). The AP-3 complex: a coat of many colours. Trends Cell Biol. *8*, 282–288.

Odorizzi, G., Katzmann, D.J., Babst, M., Audhya, A., and Emr, S.D. (2003). Bro1 is an endosome-associated protein that functions in the MVB pathway in *Saccharomyces cerevisiae*. J. Cell Sci. *116*, 1893–1903.

Pernier, J., Shekhar, S., Jegou, A., Guichard, B., and Carlier, M.F. (2016). Profilin interaction with actin filament barbed end controls dynamic instability, capping, branching, and motility. Dev. Cell *36*, 201–214.

Phin, N., Parry-Ford, F., Harrison, T., Stagg, H.R., Zhang, N., Kumar, K., Lortholary, O., Zumla, A., and Abubakar, I. (2014). Epidemiology and clinical management of Legionnaires' disease. Lancet Infect. Dis. *14*, 1011–1021.

Plouffe, J.F., File, T.M., Breiman, R.F., Hackman, B.A., Salstrom, S.J., Marston, B.J., and Fields, B.S. (1995). Reevaluation of the definition of Legionnaires' disease: use of the urinary antigen assay. Clin. Infect. Dis. *20*, 1286–1291.

Pollard, T.D. (2007). Regulation of actin filament assembly by Arp2/3 complex and formins. Annu. Rev. Biophys. Biomol. Struct. *36*, 451–477.

Purcell, M., and Shuman, H.A. (1998). The *Legionella pneumophila icmGCDJBF* genes are required for killing of human macrophages. Infect. Immun. *66*, 2245–2255.

Raymond, C.K., Howald-Stevenson, I., Vater, C.A., and Stevens, T.H. (1992). Morphological classification of the yeast vacuolar protein sorting mutants: evidence for a prevacuolar compartment in class E vps mutants. Mol. Biol. Cell *3*, 1389–1402.

Rechnitzer, C., and Blom, J. (1989). Engulfment of the Philadelphia strain of *Legionella pneumophila* within pseudopod coils in human phagocytes. Comparison with other *Legionella* strains and species. Apmis *97*, 105–114.

Rink, J., Ghigo, E., Kalaidzidis, Y., and Zerial, M. (2005). Rab conversion as a mechanism of progression from early to late endosomes. Cell *122*, 735–749.

Rolando, M., Sanulli, S., Rusniok, C., Gomez-Valero, L., Bertholet, C., Sahr, T., Margueron, R., and Buchrieser, C. (2013). *Legionella pneumophila* effector RomA uniquely modifies host chromatin to repress gene expression and promote intracellular bacterial replication. Cell Host Microbe *13*, 395–405.

Ronneberger, O., Fischer, P., and Brox, T. (2015). U-Net: convolutional networks for biomedical image segmentation. Lect. Notes Comput. Sci. LNCS - Springer *9351*, 234–241.

Rothman, J., and Söllner, T. (1997). Throttles and dampers: controlling the engine of membrane fusion. Science *276*, 1212–1213.

Rowbotham, T.J. (1980). Preliminary report on the pathogenicity of *Legionella pneumophila* for freshwater and soil amoebae. J. Clin. Pathol. *33*, 1179–1183.

Roy, C.R., Berger, K.H., and Isberg, R.R. (1998). *Legionella pneumophila* DotA protein is

required for early phagosome trafficking decisions that occur within minutes of bacterial uptake. Mol. Microbiol. *28*, 663–674.

Sadosky, A.B., Wiater, L.A., and Shuman, H.A. (1993). Identification of *Legionella pneumophila* genes required for growth within and killing of human macrophages. Infect. Immun. *61*, 5361–5373.

Segal, G., Purcell, M., and Shuman, H.A. (1998). Host cell killing and bacterial conjugation require overlapping sets of genes within a 22-kb region of the *Legionella pneumophila* genome. Proc. Natl. Acad. Sci. U. S. A. *95*, 1669–1674.

Shohdy, N., Efe, J.A., Emr, S.D., and Shuman, H.A. (2005). Pathogen effector protein screening in yeast identifies *Legionella factors* that interfere with membrane trafficking. Proc. Natl. Acad. Sci. U. S. A. *102*, 4866–4871.

Siddhanta, U., McIlroy, J., Shah, A., Zhang, Y., and Backer, J.M. (1998). Distinct roles for the p110α and hVPS34 phosphatidylinositol 3'- kinases in vesicular trafficking, regulation of the actin cytoskeleton, and mitogenesis. J. Cell Biol. *143*, 1647–1659.

Sönnichsen, B., De Renzis, S., Nielsen, E., Rietdorf, J., and Zerial, M. (2000). Distinct membrane domains on endosomes in the recycling pathway visualized by multicolor imaging of Rab4, Rab5, and Rab11. J. Cell Biol. *149*, 901–913.

Spaargaren, M., and Bos, J.L. (1999). Rab5 induces Rac-independent lamellipodia formation and cell migration. Mol. Biol. Cell *10*, 3239–3250.

Svarrer, C.W., Lück, C., Elverdal, P.L., and Uldum, S.A. (2012). Immunochromatic kits Xpect *Legionella* and BinaxNOW *Legionella* for detection of *Legionella pneumophila* urinary antigen have low sensitivities for the diagnosis of Legionnaires' disease. J. Med. Microbiol. *61*, 213–217.

Valdivia, R.H. (2004). Modeling the function of bacterial virulence factors in *Sccharomyces cerevisiae*. Eukaryot. Cell *3*, 827–834.

Vogel, J.P., and Isberg, R.R. (1999). Cell biology of *Legionella pneumophila*. Curr. Opin. Microbiol. *2*, 30–34.

Vogel, J.P., Andrews, H.L., Wong, S.K., and Isberg, R.R. (1998). Conjugative transfer by the virulence system of *Legionella pneumophila*. Science. *279*, 873–876.

Weisstein, E. W. (2019). Logistic equation. MathWorld - A Wolfram Web Resource. Retrieved from http://mathworld.wolfram.com/LogisticEquation.html on October 4, 2019.

Wiater, L.A., Dunn, K., Maxfield, F.R., and Shuman, H.A. (1998). Early events in phagosome establishment are required for intracellular survival of *Legionella pneumophila*. *66*, 4450–4460.

Winn, W.C. (1988). Legionnaires' disease: historical perspective. Clin. Microbiol. Rev. *1*, 60–81.

Witke, W. (2004). The role of profilin complexes in cell motility and other cellular processes. Trends Cell Biol. *14*, 461–469.

World Health Organization (2018). Legionellosis. World Heath Organization. Retrieved from https://www.who.int/news-room/fact-sheets/detail/legionellosis on October 4, 2019.

Zhen, Y., and Stenmark, H. (2015). Cellular functions of Rab GTPases at a glance. J. Cell Sci.

128, 3171–3176.

Zhu, W., Banga, S., Tan, Y., Zheng, C., Stephenson, R., Gately, J., and Luo, Z.Q. (2011). Comprehensive identification of protein substrates of the Dot/Icm type IV transporter of *Legionella pneumophila*. PLoS One *6*, e17638.

7. Supplementary data

Supplementary Table S1. Solutions and reagents used during the experimental work.

Buffer solution	Components
1 M $MgSO_4$	1 M $MgSO_4 \cdot 7H_2O$ (Merck) dH_2O up to the desired volume
50x 5052 solution	25% (w/v) glycerol (VWR Chemicals) 2.5% (w/v) D(+)-glucose (Carl Roth) 10% (w/v) α-lactose (Sigma) dH_2O up to the desired volume
20x NPS salts solution	6.6% (w/v) $(NH_4)SO_4$ (Merck) 13.6% (w/v) KH_2PO_4 (Merck) 14.2% (w/v) Na_2HPO_4 (Merck) dH_2O up to the desired volume
Sodium-phosphate buffer pH 8.0	50 mM Na_2HPO_4 (Merck) 300 mM NaCl (VWR Chemicals) dH_2O up to the desired volume
Imidazole 4 M stock solution pH 8.0	4 M imidazole (Merck) ddH_2O up to the desired volume
Lysis Buffer pH 8.0	Sodium-phosphate stock solution to the desired volume 20 mM imidazole
Wash Buffer pH 8.0	Sodium-phosphate stock solution to the desired volume 40 mM imidazole
Elution Buffers (100, 200, 500 mM imidazole) pH 8.0	Sodium-phosphate stock solution to the desired volume 100, 200, or 500 mM imidazole
GST-Rab5 Storage Buffer	50 mM HEPES pH 7.5 (Sigma) 50 mM NaCl (VWR Chemicals) 1 mM EDTA (Carl Roth) dH_2O up to the desired volume
1.5 M Tris pH 8.8	1.5 M Tris (Carl Roth) dH_2O up to the desired volume
1 M Tris pH 6.8	1 M Tris (Carl Roth) dH_2O up to the desired volume

5x SDS-PAGE loading buffer	0.25 M Tris-HCl pH 6.8 10% (w/v) SDS (NZYTech) 50% (v/v) glycerol (VWR Chemicals) 0.5 M β-mercaptoethanol (Sigma) 0.5% (w/v) Bromophenol blue (Scharlau) dH_2O up to the desired volume
Coomassie staining solution	40% (v/v) methanol (Merck) 7% (v/v) glacial acetic acid (Scharlau) 0.2% (w/v) Coomassie Brilliant blue (Amresco) dH_2O up to the desired volume
Distaining solution	40% (v/v) methanol 7% (v/v) glacial acetic acid dH_2O up to the desired volume
10x Tris-glycine buffer	0.25 M Tris buffer grade (Carl Roth) 1.92 M glycine (NZYTech) dH_2O up to the desired volume
Nucleotide Exchange Buffer	20 mM HEPES pH 7.5 (Fisher Bioreagents) 100 Mm NaCl 10 mM EDTA (Merck) 5 mM $MgCl_2$ (Acros Organics) 1 mM DTT (Fisher Bioreagents) dH_2O up to the desired volume
Nucleotide Stabilization Buffer	20 mM HEPES (Fisher Bioreagents) 100 mM NaCl 5 mM $MgCl_2$ (Acros Organics) 1 mM DTT (Fisher Bioreagents) dH_2O up to the desired volume
100 mM Mg-ATP	100 mM ATP (Sigma-Aldrich) 100 mM $MgCl_2$ (Acros Organics) dH_2O up to the desired volume
G-buffer	1 mM Tris-HCl pH 7.8 or 8.0 0.2 mM $CaCl_2$ (PanReac) 0.5 mM DTT (Fisher Bioreagents) 0.2 mM Mg-ATP dH_2O up to the desired volume
10x ME buffer	4 mM $MgCl_2$ (Acros Organics) 20 mM EGTA (Merck) dH_2O up to the desired volume

10x KMEI buffer pH 7.0	500 mM KCl (PanReac) 20 mM $MgCl_2$ (Acros Organics) 20 mM EGTA (Merck) 300 mM imidazole (SERVA) dH_2O up to the desired volume
Imaging Buffer	40 μg/ml catalase from bovine liver (SERVA) 1.8 mg/ml glucose oxidase from Aspergillus niger (SERVA) 100 mM α-D-glucose (SERVA) 2.5% 2-mercaptoethanol (Fisher Bioreagents) 0.5% methylcellulose (Sigma-Aldrich)

Supplementary Table S2. Plasmids and vectors used during the experimental work.

Plasmid/Vector	Characteristics	Reference
pET15b-vipA	His_6-$VipA_{WT}$ encoded in pET15b (pET derivative, Novagen)	Franco et al., 2012
pIF415	GST-$Rab5_{WT}$ encoded in pGEX-4T-2	Franco et al. (unpublished)
pIF416	GST-$Rab5_{CA}$ encoded in pGEX-4T-2	Franco et al. (unpublished)
pEF6/Myc-His A	Mammalian Expression Vector	Life Technology
pIF328	$VipA_{WT}$-myc encoded in pEF6/Myc-His A	Bugalhão et al., 2015

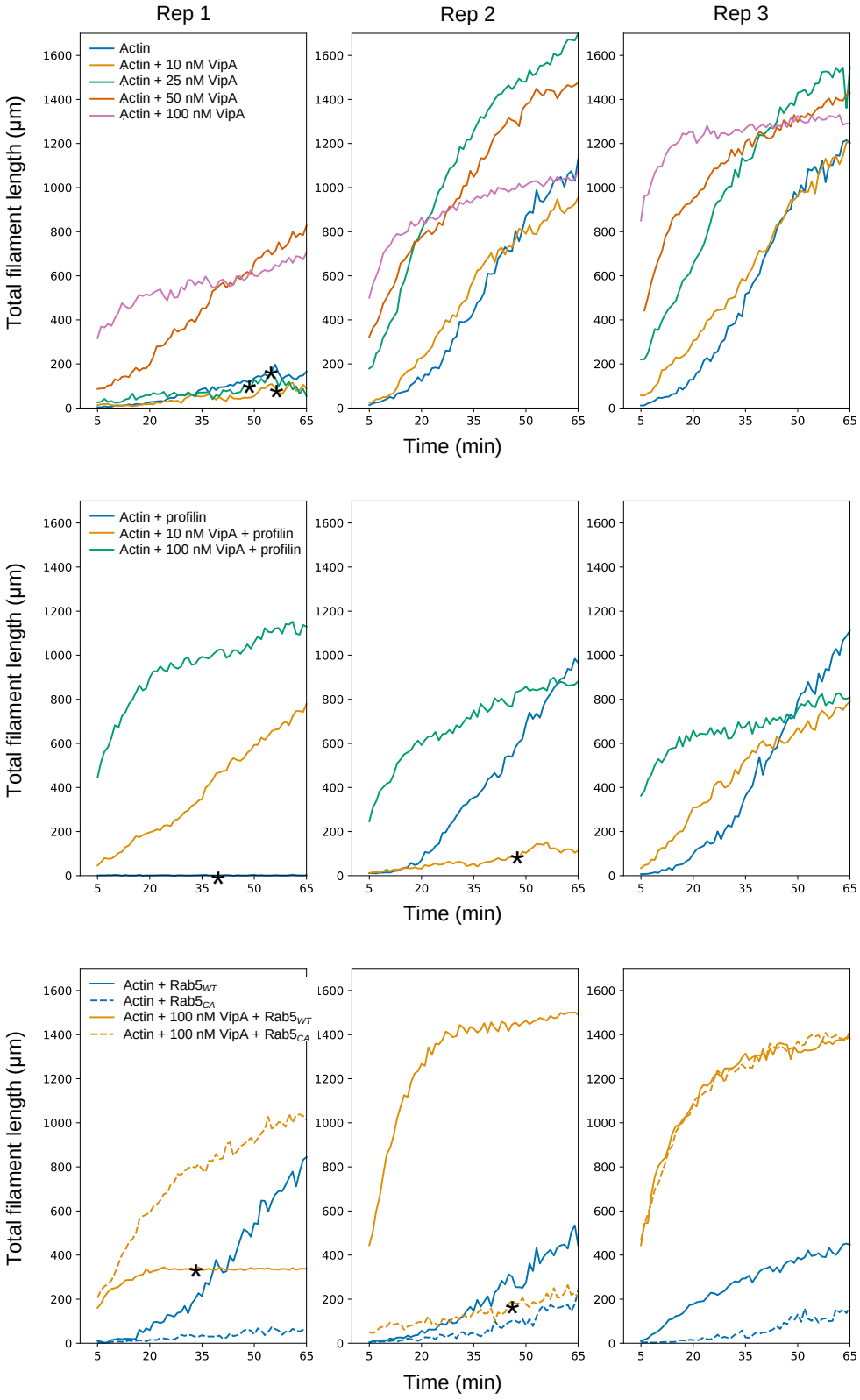

Supplementary Figure S1. Individual replicates of actin polymerization over time. Samples contained 100 nM of Atto 488-monomeric actin and the displayed VipA concentrations. In the corresponding cases, 700 nM of profilin or 100 nM of Rab5 (wild type or constitutively active mutant) were added to the sample. Curves correspond to total filament length over time. Displayed asterisks correspond to samples in which

total filament length did not achieve at least 50% of the maximum verified in other replicate for the same condition. These data were considered as outliers and excluded from analysis.

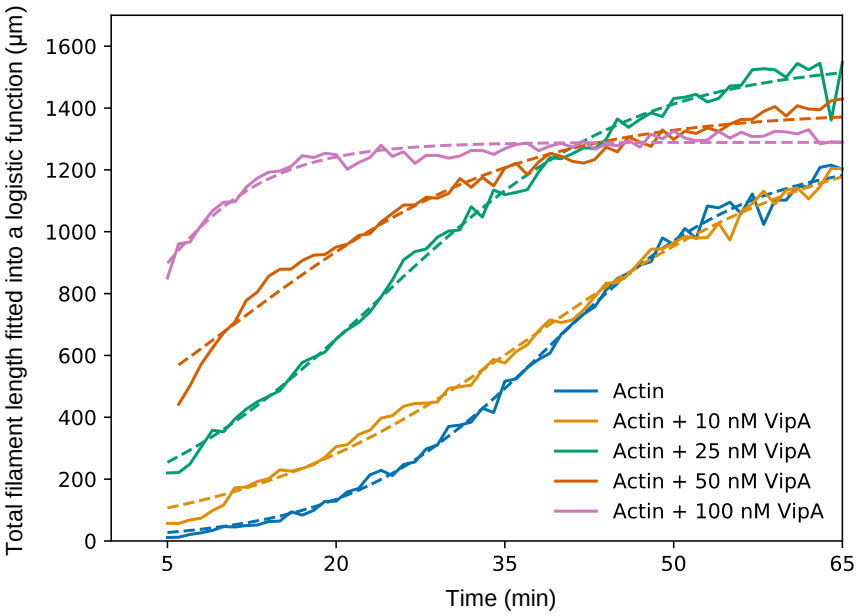

Supplementary Figure S2. Fitting of total filament length over time into a logistic function defined by the parameters τ, *m* and *k*. Curves correspond to the third experimental replicate of actin polymerization assays in the presence of the displayed VipA concentrations. Fitting into a logistic function described by a sigmoidal curve was done using a least squares regression.